Journal of Materials Chemistry A

Accepted Manuscript

ROYAL SOCIETY OF CHEMISTRY

www.rsc.org/materialsA

Journal of Materials Chemistry A

ARTICLE

Counter electrode materials combined with redox couples in dye- and quantum dot-sensitized solar cells

Received 00th January 20xx,
Accepted 00th January 20xx

DOI: 10.1039/x0xx00000x

www.rsc.org/

Mingxing Wu,*[a] Xiao Lin,[b] Yudi Wang,[c] and Tingli Ma*[d]

Dye- or quantum dot-sensitized solar cells (DSCs or QDSCs) comprise a sensitizer, a semiconductor, an electrolyte containing redox couple, and a counter electrode (CE), which have inspired a new wave of research. The challenges in realizing the practical application of such photovoltaic devices are the enhancement of photovoltaic performance, stability, and the reduction of fabrication costs. The CE is an important component, and the exploration of low cost CE catalysts to match the redox couples has become a feasible route in the pursuit of high PCE and low production cost of the devices. This article reviews the development of ~~low-cost~~ CE catalysts for the regeneration of each type of iodide-free redox couple, including inorganic, organic, and transition metal complex-based redox couples, among others.

Introduction

Continuously growing world energy consumption and environmental problems drive our search for alternative renewable energy sources. Fortunately, the sun provides us with an inexhaustible source of solar energy. Solar cells are photovoltaic devices in which sunlight is converted into electricity. In the last few decades, photovoltaic production has maintained a high growth rate of over 20%, making it the fastest growing energy conversion technology.[1] Although the photovoltaic industry is presently dominated by silicon-based solar cells, enthusiasm for the development of new types of solar cells is very high. Among these, dye- and quantum dot-sensitized solar cells (DSCs, QDSCs) are of particular interest. These photovoltaic devices commonly contain three components: a photoanode (sensitizer absorbed on the surface of semiconductor), an electrolyte (containing a redox couple) or hole transport material (HTM), and a counter electrode (CE). The acknowledged merits of DSCs include environmental friendliness, transparency, good plasticity, ease of building combination and a simple fabrication procedure. Currently, laboratory-scale DSCs have reached power conversion efficiencies (PCE) of ~13% under standard conditions, while the efficiency generated by larger modules is 9.9%.[2] In a word, DSCs provide a promising alternative to conventional p–n junction photovoltaic devices. Based on the structure of DSCs, quantum dots have been introduced as an alternative to dyes, resulting in so-called QDSCs.[3] Very recently, the record PCE value of QDSCs jumped to over 8.21%.[4]

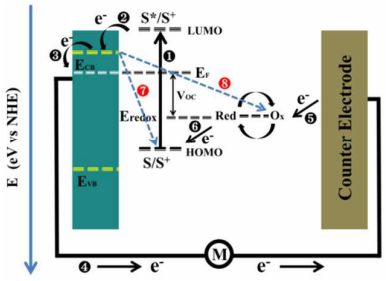

Fig. 1 Electricity generating principle of the DSCs.

DSCs were the original models of this type of photovoltaic devices, carried forward by Michael Grätzel et al. through the introduction of the mesoporous TiO_2 semiconductor film.[5] These devices simulate the photosynthesis which has occurred naturally for over 3.5 billion years; this technology is therefore often described as "artificial photosynthesis".[6a] Fig. 1 depicts the electricity generating principle of DSCs. Under illumination, a sensitizer molecule (S) jumps to an excited state (S*), and the unstable S* releases a photoelectron (e^-) into the conduction band (CB) of the semiconductor, leaving behind a sensitizer hole (S^+). Next, the photoelectrons in the CB are collected by the substrate, flow through the external circuit, and reach the CE. The oxidation state of the redox couple (Ox) is reduced to

[a] College of Chemistry and Material Science, Hebei Normal University, No. 20 Rd. East of 2nd Ring South, Yuhua District, Shijiazhuang City, Hebei Province, P. R. China, Tel. & Fax:+86-311-80787438, E-mail: mingxing@mail.ustc.edu.cn
[b] Shanghai Institute of Applied Physics, Chinese Academy of Sciences Jialuo Road 2019, Shanghai, 201800, P. R. China
[c] State Key Laboratory of Inorganic Synthesis and Preparative Chemistry, College of Chemistry, Jilin University
[d] Graduate School of Life Science and Systems Engineering, Kyushu Institute of Technology, 2–4 Hibikino, Wakamatsu, Kitakyushu, Fukuoka 808–0196, Japan E-mail: tinglima@dlut.edu.cn.
Electronic Supplementary Information (ESI) available: [Table S1-S8 summarized the photovoltaic parameters]. See DOI: 10.1039/x0xx00000x

the reduction state (Red) by the electrons at the CE. Meanwhile, S^+ is regenerated by Red, which is oxidized to Ox at the same time, completing the circuit. The electron transfer process is always accompanied by electron recombination: the recombination process occurs between the photoelectrons and S^+ or Ox. Recombination is a major cause of efficiency loss in DSCs.

The realization of commercial applications for DSCs (or QDSCs) requires a substantive increase of the PCE and a drastic decrease in the production cost. The design of sensitizers with a broad absorption band seems to be the key path to improving the PCE. The open-circuit voltage (V_{oc}) of the device is determined by the gap between the quasi-Fermi level (E_F) of the electrons in the oxide under illumination and the redox potential of the electrolyte (E_{redox}). A redox couple with higher potential provides a higher V_{oc} and a powerful path to higher PCE, and more information about redox couples is available in a previous review article.[6] In DSCs (or QDSCs), the CE functions as a catalyst or hole extractor, responsible for the regeneration of the redox couple, and requiring the advantages of high catalytic activity toward the selected redox couple, high electronic conductivity, low cost, and good stability during long-term use. In addition to the conventional Pt CE, carbon materials, transition metal compounds and polymers can be used as CE catalysts. Studies have found that CE catalysts and redox couples closely relate to each other, a matching issue between them.[7] This suggests that we should re-consider the role of CE catalysts toward a fixed redox couple in the pursuit of high PCE values. Furthermore, the development of ~~low cost~~ Pt-free CE catalysts is a promising path to the reduction of production costs by replacing expensive Pt CE. The exploration of low cost CE catalysts for fixed redox couples is therefore of great interest, and here we summarize the recent progress in CE catalysts combined with iodide-free redox couples.

2. Counter electrode (CE) catalysts in dye-sensitized solar cells (DSCs)

2.1 CE Catalysts for inorganic iodide-free redox couples

In DSC systems, I^-/I_3^- is the prevalent redox couple because the iodide electrolyte has desirable kinetic properties that meet the requirements of "asymmetric behaviour" in the DSCs: the forward electron donation by I^- diffuses rapidly to guarantee efficient dye regeneration while the recombination of I_3^- with the electron in the photoanode is inactive for high carrier collection efficiency. Pt was first used to catalyze the regeneration of the I^-/I_3^- redox couple and the mechanism of the I_3^- reduction at the Pt/electrolyte interface has been thoroughly investigated.[8] Because of the high cost and limited reserves of Pt, many Pt-free CE catalysts have been applied to replace Pt, such as carbon materials, polymers, inorganic materials, multiple compounds, composites, etc.[9] In terms of redox couples, the I^-/I_3^- based electrolyte has obvious shortcomings which cannot keep up with the ongoing advancements of DSCs. First, the iodide electrolyte absorbs short wavelength light, resulting in lower short circuit current density (J_{sc}) and PCE. Second, I_3^- corrodes Ag and Cu electron collectors. Third, the sublimation of I_2 is a potential threat to the long-term use of DSCs. Moreover, the mismatch (approximately 0.6 eV) between the redox potential of a typical sensitizer ($E_{F,redox}$≈1.0 eV vs. NHE) and that of I^-/I_3^- ($E_{F,redox}$≈0.4 eV vs. NHE) leads to a V_{oc} loss. To overcome these shortcomings, alternatives to I^-/I_3^- are being developed, including other inorganic, organic, and transition metal complex-based redox couples. In addition to I^-/I_3^-, inorganic redox couples include Br^-/Br_3^-, $SCN^-/(SCN)_3^-$, etc. Br^-/Br_3^- presents a high positive redox potential of 1.1 V vs. NHE. Furthermore, the Br^-/Br_3^-electrolyte absorbs much less visible light than the I^-/I_3^- electrolyte. Sun et al. applied the Br^-/Br_3^- redox couple in DSCs with dyes of TC301 and TC306, which produced PCE values of 3.7 and 5.2% with high V_{oc} values of 1.16 V and 0.94 V, respectively.[10] Meyer et al. reported that the pseudohalide redox couples of $SCN^-/(SCN)_3^-$ and $SeCN^-/(SeCN)_3^-$ also had more positive redox potentials than I^-/I_3^-; however, the original performance of the pseudohalide was very disappointing. The highest incident photocurrent conversion efficiency (IPCE) values of $SCN^-/(SCN)_3^-$ and $SeCN^-/(SeCN)_3^-$ based DSCs are only 4 and 20%, much lower than that of I^-/I_3^-based DSCs under the same conditions. This is likely due to the inefficient regeneration of the N3 dye by these types of pseudohalide redox couples.[11] Grätzel and co-workers developed ionic liquid electrolytes using the $SCN^-/(SCN)_3^-$ redox couple for high-efficiency DSCs which produced unprecedented PCE values of 7.5–8.3%.[12] In the aforementioned work, Pt was used as the CE catalyst for Br^-/Br_3^- and the pseudohalide redox couples. Sun et al. Prepared the sulfide redox couple of $((CH_3)_4N)_2S/((CH_3)_4N)_2S_2$ with good solubility in organic solvents. Based on an organic dye (TH305), the DSCs yielded a PCE of 5.24% with a CoS CE. The same DSCs using a Pt CE gave a PCE of 4.55%.[13] The higher catalytic activity of CoS over Pt toward $((CH_3)_4N)_2S/((CH_3)_4N)_2S_2$ can be ascribed to the lower charge transfer resistance (R_{ct}) and series resistance (R_s) of the CoS CE. The experimental conditions and results from the inorganic iodide-free redox couple-based DSCs using different counter electrode catalysts are summarized in Table S1.

Halide and pseudohalide redox couples are the widely used iodide-free inorganic redox couples in DSCs and Pt is the dominant CE catalyst. There are few reports on Pt-free catalysts with iodide-free inorganic redox couples.

2.2 CE Catalysts for organic redox couples

In addition to the inorganic redox couples, another important and fashionable redox couple family is the organic compounds, including 2,2,6,6-tetramethyl-1-piperidinyloxy ($TEMPO/TEMPO^+$), phenothiazine (PTZ/PTZ^+), tetraphenyl-diamine (TPD/TPD^+), hydroquinone/benzoquinone (HQ/BQ), thiolate/disulfide, etc.[14] Compared to the inorganic redox couples, the organic redox couples have the following merits: (1) diversity of the redox couples, (2) easy modification of the molecule and the subsequent redox potential, (3) colorless organic redox electrolytes. Based on these merits, organic

redox couples have great potential to replace inorganic redox couples.

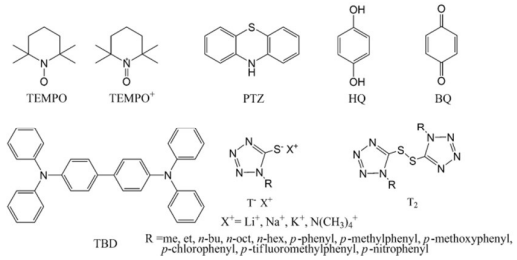

Fig.2 Molecular structure of the organ redox couples of TMEPO, PTZ, TBD, HQ/BQ, and T^-/T_2.

In 2006, M. Grätzel et al. employed a stable organic radical, TEMPO) and its oxide state ($TMEPO^+$) as the redox couple in DSCs.[14a] The standard redox potential of TEMPO/$TEMPO^+$ was approximately 0.8 V vs. NHE, 0.4 V higher than the conventional I^-/I_3^-. Combined with an organic dye (D149) with matched energy levels and the traditional Pt CE, the device showed an expected high V_{oc} of 0.83 V and a PCE of 5.4%. The relatively low PCE value can be ascribed to the short electron lifetime due to the recapture of photoelectrons from the photoanode, accomplished much faster by $TEMPO^+$ than I_3^-, which leads to a low photovoltage and photocurrent. PTZ has a smaller reorganizational energy associated with the electron transfer and is thus considered for co-redox couples. Bignozzi et al. used PTZ and Co-complex as the co-redox couple in DSCs. Combined with the dye Z907 and a Pt CE, the device generated a PCE of 1.44% with a V_{oc} of 0.673 V.[14b] As a well-known hole conductor, TPD has also been introduced into DSCs. The TPD/TPD^+ redox couple has a large redox potential of 1.095 V vs. NHE. N3 sensitized DSCs with Pt CE produced a low PCE<1% with a high V_{oc} of 0.9 V.[14c,d] HQ is a very robust reductant and can lose two electrons, forming BQ. The redox potential of HQ/BQ is more positive than that of I^-/I_3^- but more negative than the HOMO level of most sensitizers, indicating that HQ/BQ is a promising redox couple for DSCs in pursuit of higher V_{oc} and PCE. Sun et al. investigated the impact of various CEs on HQ/BQ electrolyte-based DSCs.[14e,f] For the N719-based DSCs, the application of poly(3,4-ethylenedioxythiophene) (PEDOT) and MWCNTs CEs showed PCEs of 5.2 and 4.9%, respectively, higher than that of the device using the traditional Pt CE (4.7%). Similarly, for the organic dye CM309 sensitized DSCs, the devices using PEDOT and MWCNTs CEs also behaved better than Pt. This result indicates that Pt-free catalysts are much more suitable for the regeneration of the HQ/BQ redox couple. As the HQ/BQ electrolyte is not stable, few subsequent reports about the HQ/BQ redox couple or the CE catalysts can be found. The experimental conditions and results of the above-mentioned organic redox couple-based DSCs using different counter electrode catalysts are summarized in Table S2.

In 2010, the Grätzel group first introduced thiolate/disulfide (T^-/T_2) as a redox couple in DSCs, where T^- represents the 5-mercapto-1-methyltetrazoleion and T_2 stands for its dimer.[14g] Fig. 2 shows the molecular structure of T^-, X^+, T_2, where the substituent R can be Me, Et, *n*-Bu, *n*-Oct, etc. and X^+ can be $N(CH_3)_4^+$, Li^+, Na^+, and K^+. The redox potential of T^-/T_2 (R=Me, X^+=$N(CH_3)_4^+$) is 0.485 V vs. NHE. With a Pt CE, the DSCs using T^-/T_2 showed a PCE of 6.48%. In the following years, T^-/T_2 derivative redox couples were introduced into DSCs. In this process, it was found that some Pt-free CE catalysts were more suitable for the regeneration of the T^-/T_2 redox couples. M. Grätzel compared the conventional Pt to CoS and PEDOT CEs for the T^-/T_2 redox couple. Using N719 dye and a PEDOT CE, the device produced a PCE of 6.9%. Replacing the N719 dye with Z907 dye, the PCE increased to 7.9%.[14h]

We have introduced carbon materials, transition metal carbides, nitrides, oxides, sulfides, phosphides, and composites into the T^-/T_2 redox couple.[7] As the carbides performed better in iodide redox couple,[9d] we first used TiC, VC, and Cr_3C_2 nanoparticles to catalyze the regeneration of the T^-/T_2 redox couple.[7a] As we expected, all of the carbide CEs brought clear advantages to the T^-/T_2 electrolyte. The corresponding DSCs showed high PCEs of 4.96 (TiC), 4.06 (VC), and 4.54% (Cr_3C_2). Compared with the Pt CE based DSCs, the PCE values were significantly improved by 35.5, 10.9, and 24.4%, respectively. The nitrides, oxides, sulfides, and phosphides have also been introduced into the T^-/T_2 system, and all of the Pt-free catalysts showed higher activity than Pt.[7c-f] In addition, the effect of the morphologies of the CE materials on catalytic activity in the applied T^-/T_2 redox couple have been investigated. The prepared Mo_2C nanotubes (Mo_2C-NTs) gave an impressive catalytic activity compared to the Mo_2C nanoparticles (Mo_2C-Ps).[7b] Electrochemical impedance spectroscopy (EIS) measurements revealed that the R_{ct} of the Mo_2C-NTs was 0.8 Ω, which was much lower than in the Mo_2C-Ps (2.0 Ω). Moreover, the Mo_2C-NTs showed low diffusion impedance (Z_N) values relative to the Mo_2C-Ps, stemming from the mesoporous structure of the Mo_2C-NTs as shown in the TEM images (Fig. 3a, b). Both the R_{ct} and Z_N proved that the redox reaction between T^- and T_2 occurs easily on the Mo_2C-NTs electrode. Similarly, the VN "peas" showed higher catalytic activity than VN cubes.[7c] The possible reasons are summarized as follows: (1) as depicted in Fig. 3c and d, VN "peas" have a smaller average particle size as well as a larger BET surface area, providing a large number of catalytic sites; (2) the different electron structures depends on the particle shape and size, leading to different catalytic activities;[15a] (3) previous studies have noted that the catalyst with smallest particle has the highest activity because of the d-band change.[15b]

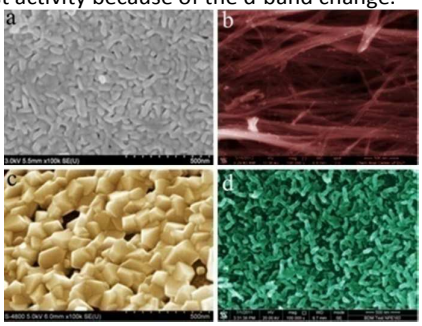

Fig. 3 SEM images of Mo_2C (a) nanoparticles, (b) nanotubes, VN (c) cubes, and (d) peas.[14c]

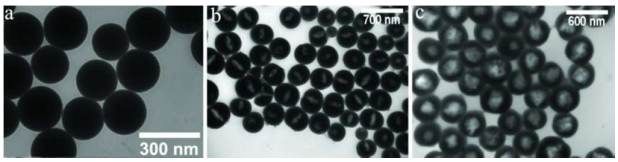

Fig. 4 TEM images of the (a) solid, (b) open-ended, and (c) hollow carbon sphere.[16a]

In addition to the transition metal compounds, carbon is also a promising CE catalyst for DSCs because of its high catalytic activity, low cost, ready accessibility, excellent thermal stability and corrosion resistance. Traditional carbon materials, such as activated carbon (Ca), carbon black (Cb), carbon dye (Cd), and mesoporous carbon (MC) have been previously used for the T^-/T_2 redox couple.[14d,g] The DSCs based on these carbon CEs produced respective PCE values of 4.96, 5.05, 4.75, and 4.60%. All of the carbon materials behaved better than Pt for the T^-/T_2 redox couple. Recently, a new type of carbon sphere (denoted as OCS) with an open end on the surface was introduced into DSCs for the T^-/T_2 redox couple.[16a] The OCS CE fabricated in N_2 atmosphere showed higher catalytic activity than the conventional solid and hollow carbon sphere CEs, indicating its potential to replace expensive Pt CE. The OCS CE based DSCs produce a high PCE of 6.4%, much higher than that of Pt CE based DSCs (4.1%). The high catalytic activity of OCS stems from the sufficient contact between the redox couple and the external and internal surfaces of the OCS because of its open end, which provides a diffusion channel for the electrolyte into the inside of the OCS. Lin et al. arranged single-walled carbon nanotubes (SWCNTs) onto FTO glass vertically by a transfer technique. This CNTs CE featured remarkably stronger catalytic activity toward T^-/T_2 redox couple than Pt CEs.[16b] After optimization, the device using this CNTs CE produced a PCE of up to 5.25%, which was significantly higher the Pt CE based DSCs. Further, Peng et al. fabricated wire type DSCs using CNTs CEs combined with T^-/T_2 redox couple.[16c] The flexible wire device achieved a maximal PCE of 7.33%, again much higher than the PCE value of 2.06% for the Pt CE based DSCs. Interestingly, this type of DSC using a T^-/T_2 redox couple surpassed the conventional I^-/I_3^- redox couple based DSCs. The Zou group assembled DSCs with integrated graphite CEs, which worked as the substrate as well as the catalyst, combined with the T^-/T_2 redox couple. The device showed a PCE of 4.79%, also higher than the Pt CE based DSCs (3.97%).[16d]

Several carbonaceous materials have been used as CEs in DSCs. To further improve their catalytic activity, composites were used in which carbon materials were often the supporter due to their high stability and large surface area. We synthesized composites of VC-MC, WC-MC, Ni_5P_4-MC, and WO_2-MC, where MC was the supporter and the carbides, oxide, and phosphide were the catalysts, then introduced the composites into DSCs for the regeneration of the T^-/T_2 redox couple.[14a,d,f,g] All of the composites showed higher catalytic activity than Pt and the very high catalytic activity of the composites can be explained as follows: (1) the intrinsic high catalytic activity of catalysts, (2) the synergistic catalytic effect of catalyst and supporter, (3) the improved conductivity stemming from the MC, (4) the large porosity of the composites which is beneficial to electrolyte diffusion. Zhang et al. Utilized Cb as a supporter and several conductive polymers as catalysts to make composite CEs for the T^-/T_2 electrolyte.[17] Specifically, they polymerized pyrrole (Py), aniline (ANI), and 3,4-ethylenedioxythiophene (EDOT) on a Cb film which was then screen printed on FTO glass to form Cb/polypyrrole (PPy), Cb/Polyaniline (PANI), and Cb/PEDOT composites for the T^-/T_2 redox couple. The corresponding DSCs showed PCE values of 5.2 (Cb/PPy), 5.2 (Cb/PANI), and 7.6% (Cb/PEDOT). The photovoltaic discrepancies are rooted in the fill factor (FF), which determined the PCE partly. The FF of a bare Cb CE is only 0.31. After loading PPy, PANI, and PEDOT on the Cb film, the FFs were increased to 0.49, 0.46 and 0.70, respectively. The experimental conditions and results of the organic T^-/T_2 (R=me) redox couple based DSCs using different counter electrode catalysts are summarized in Table S3.

The above-mentioned organic redox couples were all T^-/T_2, and the R group was methyl. The champion device based this organic redox couple gave the highest PCE of 7.6%. However, the V_{oc} values of the T^-/T_2 based DSCs are all less than 0.7 V due to the substantially negative redox potential (E_{redox}) of T^-/T_2 relative to the Fermi levels of the anode semiconductor, thus posing a barrier to further improvement of the PCE. To solve this problem, Han et al. used DFT calculations to design a group of sulfide redox couples by introducing electron-donating and-withdrawing groups to the T^- backbone.[18a] As shown in Fig. 2, the R groups include *p*-phenyl, *p*-methylphenyl, *p*-methoxyphenyl, *p*-chlorophenyl, *p*-tifluoromethylphenyl, and *p*-nitrophenyl. The values of E_{redox} were tuned in the range of 0.32 to 0.49 V vs. NHE and the V_{oc} of the devices were 0.620 to 0.715 V. When the R group was *p*-methoxyphenyl, the sulfide redox couple gave the best electrochemical behavior. However, the conventional Pt CE showed poor catalytic activity toward all of the modified sulfide redox couples and the corresponding DSCs produced PCE values lower than 1%. The authors found that all of the T^-/T_2 redox couples are much more compatible with carbon CEs than Pt CEs. Furthermore, the authors prepared a novel graphene modified CE called GGCM, resulting in higher PCE values of 5.65 (R=*p*-phenyl), 5.90 (R=*p*-methylphenyl), 6.14 (R=*p*-methoxyphenyl), 3.76 (R=*p*-chlorophenyl) 3.14 (R=*p*-tifluoromethylphenyl), and 3.25% (R=*p*-nitrophenyl). Note that the redox couples with electron-donating groups behaved better than those with electron-withdrawing groups. After optimizing the concentration of the oxide state of the redox couple, the DSCs with T^-/T_2 (R=*p*-methoxyphenyl) and a GGCM CE gave the highest PCE of 6.53%. In addition, they applied two types of PEDOT CEs ($PEDOT_{UT}$, $PEDOT_{BE}$) for the modified T^-/T_2 redox couple, where R= *p*-phenyl, and the DSCs produced high PCE values of 6.07 ($PEDOT_{UT}$) and 4.57% ($PEDOT_{BE}$).[18b] Importantly, the $PEDOT_{BE}$ showed a high transparency>91%, and the DSCs showed a high PCE of 4.35% from rear-side irradiation.

Transparent NiS CEs were electrodeposited by the facile periodic potential reversal (PR) technique in 1 period (denoted as NiS_{PR1}) for the T^-/T_2 redox couple where R=et.[18c] The NiS_{PR1} CE showed a high transparency of 90% and the DSCs yielded a PCE of 6.25%, higher than the Pt CE based DSCs (3.98%). The high catalytic activity, transparency, and low temperature methods make this NiS_{PR1} CE of great potential in bifacial, flexible and transparent DSCs when combined with the sulfide electrolyte. Further, a graphene modified mesoscopic carbon (GMC) CE was introduced for this type of redox couple, and a high PCE of 6.55% has been obtained for the corresponding DSCs, which was an increase of 35% over the analogous DSCs using a mesoscopic carbon CE (4.82%); both carbonaceous materials perform better than Pt.[18d] Funabiki et al. also prepared T^-/T_2 redox couples with long alkyl R groups such as *n*-Bu, *n*-Hex, and *n*-Oct. With a PEDOT CE, the DSCs employing these organic sulfide redox couples gave optimized PCE values of 4.25 (R=*n*-Bu), 4.32 (R=*n*-Hex), and 3.61% (R=*n*-Oct). The lower efficiency behavior of the redox couple (R=*n*-Oct) stems from the increased resistance of electrolyte diffusion in the DSCs.[18e] The experimental conditions and results of the organic of T^-/T_2 (R=other units) redox couples based DSCs using different counter electrode catalysts are summarized in Table S4.

The above-mentioned T^-/T_2 redox couples are based on the tetrazole frame, differentiated by R groups, and investigations have been performed to study the impact of the R group on the electrochemical properties of the T^-/T_2 redox couples and the impact of the CE catalytic materials for the T^-/T_2 redox couples. Based on 2-mercapto-5-methyl-1,3,4-thiadiazole (McMT), Sun et al. prepared a class of $McMT^-X^+$/BMT (Fig. 5) redox couples, where X^+ can be TBA^+, EMI^+, and $DMHI^+$.[19] The redox potential of $McMT^-$/BMT (X^+=TBA^+) was 0.155 V vs. NHE. After optimization, the device using this redox couple and a Pt CE produced a PCE of 5.1% with a high V_{oc} of 0.774V, rivalling the iodide redox couple based DSCs. EIS measurements revealed that the main reason for the lower PCE value can be attributed to the considerably higher R_{ct} at the CE, leading to low FF and PCE values. This indicates that Pt is not an efficient catalyst for the reduction of BMT.[19a] To solve this problem, they introduced a PEDOT CE for the $McMT^-$/BMT (X^+=TBA^+) redox couple, and the device gave a PCE of 6.0%.[19b] As the X^+ is changed to EMI^+, $DMHI^+$ while the two thiolates are pure ionic liquids at room temperature. Thus, the researchers dissolved 0.2 M BMT in the two ionic liquids to obtain solvent-free T^-/T_2 electrolytes, named IL1 and IL2. The devices using these IL electrolytes and PEDOT CEs produced PCE values of 0.7 (IL1) and 0.1% (IL2) under a light intensity of 1 sun. However, the PCE increased remarkably to 3.4 (IL 1) and 0.8% (IL) when the light intensity decreased to 0.1 sun. These results imply that the mass transport of the BMT in the IL electrolytes plays an important role with respect to the disappointing FF and PCE values which are likely caused by the low catalytic activity of the PEDOT CE or diffusion resistances in the electrolyte, have been confirmed by the EIS results. Furthermore, four modified T^-/T_2 redox couples were synthesized: A^-/A_2, B^-/B_2, C^-/C_2, and D^-/D_2, as shown in Fig. 5. A^-/A_2, C^-/C_2, and D^-/D_2 showed similar structures with $McMT^-$/BMT by changing the S atom to O in the molecular framework. The redox potentials were determined to be 0.25 (A), 0.37 (B), 0.01 (C), and 0.29 V (D) vs. NHE. Combined with a Pt CE, the DSCs yielded PCE values of 3.3 (A), 0.6 (B), 0.2 (C), 1.6% (D).

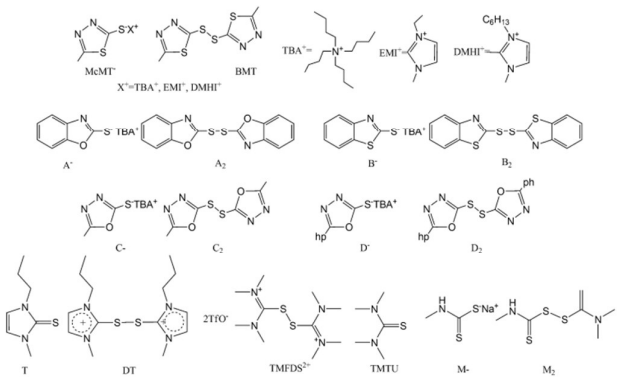

Fig. 5 Molecular structures of the T^-/T_2 derivatives.

Ghaddar et al. developed a new organic redox couple using 1-methyl-3-propylimidazole-2-thione (T) and 2,2'-dithiobis (1-methyl-3-propyl-2-imidazolinium) ditriflate (DT).[20] As shown in Fig. 5, the redox couple was presented as T/DT^{2+}. The redox potential of T/DT^{2+} was 0.62 V vs. NHE, 0.2 V more positive than the conventional I^-/I_3^- redox couple. This implies a theoretical increase in the V_{oc} of 0.2 V compared to the I^-/I_3^- electrolyte based device, which should provide a comparable regeneration rate of the oxidized sensitizer and a comparable recombination rate for the photoelectron with DT^{2+} and the oxide state of the sensitizer. The behavior of different CE catalysts on this redox couple was further investigated. MWCNTs and CoS CEs showed better catalytic activity than Pt towards the regeneration of the T/DT^{2+}. The DSCs showed PCEs of 4.12 (MWCNTs) and 3.99% (CoS), higher than the Pt CE based DSCs (2.80%). The highest catalytic activity of MWCNTs can be attributed to the high surface area. In addition, the R_{ct} values were 10, 15.4, and 37.8 Ω cm^2 for MWCNTs, CoS, and Pt, respectively. As early as 2010, Meng et al. used tetramethylthiourea (TMTU) and its oxidized dimer tetramethylformaminium disulfide dication ($TMFDS^{2+}$) to prepare a $TMTU/TMFDS^{2+}$ redox couple.[21a] They found that a Cb CE on FTO glass outperformed Pt for this type of redox couple, and the DSCs with N3 dye gave PCE values of 3.1 (Cb) and 0.6% (Pt). Furthermore, they deposited Cb films on Al and SS substrates, and both of the two CEs exhibited relatively good performance. The stability test showed that the two metals were stable in $TMTU/TMFDS^{2+}$ electrolyte. The authors attributed the efficient behavior of Cb to the high surface area of the porous carbon film as well as the corrosive resistance toward the $TMTU/TMFDS^{2+}$ electrolyte. Subsequently, Wang et al. used Z907 and D131 to replace the N3 dye for the $TMTU/TMFDS^{2+}$ based DSCs, which produced PCE values of 2.08 (Z907) and 3.88% (D131) with the help of a Cb CE.[21b] The different performance of the devices using Z907 and D131 may result from the different sensitizer regeneration rates. Kang et

al. designed a new thiolate/disulfide redox couple (M^-/M_2, Fig. 5). Using a Pt CE, the DSCs yielded a lower PCE of 0.3%. To improve the device performance, they combined the M^-/M_2 with T^-/T_2 to make binary redox couples of M^-/T_2 and T^-/M_2.[22] The PCE values of Pt CE based devices using M^-/T_2 and T^-/M_2 redox electrolytes were improved to 2.3 and 0.8%, respectively. With the Cb CE, the PCE values were further improved to 4.1 and 2.9%. Furthermore, the Cb CE showed much better stability in M^-/T_2 based DSCs compared to the traditional Pt CE. The experimental conditions and results of the above-mentioned organic redox couple based DSCs using different counter electrode catalysts are summarized in Table S5.

In summary, the lower light absorption of organic sulfide redox electrolyte is advantageous over the iodide redox electrolyte. This advantage is promising in the practical application of the transparent, organic solvent based, non-corrosive electrolytes and flexible devices. Moreover, the Pt-free CE catalysts were found more suitable to the thiolate/disulfide redox couples. For the Pt CE, the Pt particles deposited on the FTO layer are very limited and the Pt compact layer is too thin to be contacted. Iodide redox couples with small molecule size can make sufficient contact with the Pt particle, thus allowing the Pt to catalyze the iodide redox couple regeneration effectively. In contrast, for the thiolate/disulfide redox couples, the large molecules cannot make sufficient contact with the Pt particle, and the Pt therefore presents "lower" catalytic activity. For the Pt-free catalysts, the thiolate/disulfide redox couples can make sufficient contact with the large scale and mesoporous structured catalysts, inducing a high catalytic activity. Finally, the thiolate/disulfide based DSCs showing the highest PCEs are still lower than the iodide electrolyte based DSCs, leaving room to optimize the thiolate/disulfide by inhibiting recombination, improving stability, and tuning E_{redox}.

2.3 CE Catalysts for transition metal complex redox couples

As one-electron redox couples, transition metal complexes are promising alternatives to the iodide redox couples for DSCs system due to their reversible electrochemical properties, such as weak absorption towards visible light, little aggressive to metal electrodes, and easily tuned redox potential through changing the central metal atom or the ligand. The metal complexes contain Iron (Fe), copper (Cu), nickel (Ni), manganese (Mn), vanadium (V), and Cobalt (Co) complexes (Fig. 6). Among these transition metals, Fe is the cheapest one and ferrocene/ferrocenium ($FeCp_2^{0/+}$) is the most common redox couple.[23] Gregg et al. reveal that, as compared with iodide system, the $FeCp_2^{0/+}$ redox couple give higher dark current with N3 sensitized work anode, indicating a limited photovoltaic properties of DSCs using $FeCp_2^{0/+}$ redox couple and Pt CE.[13c] Hupp and co-workers introduced chlorine atoms into $FeCp_2^{0/+}$, obtaining the redox couples of $Fe(ClCp)_2^{0/+}$ and $ClCpFeCp^{0/+}$, the redox potentials of $Fe(ClCp)_2^{0/+}$ and $ClCpFeCp^{0/+}$ are more positive than $FeCp_2^{0/+}$. However, the highest PCE is still lower than 1% using the Ru based sensitizer and Pt CE.[23a] Bach et al. combined $FeCp_2^{0/+}$ redox couple with an organic dye named Carbz-PAHTDTT to fabricated DSCs. Using Pt CE, the DSCs reached a high V_{oc} of 0.842 V and an impressive PCE of 7.5%.[23b] Relative to the above organic electrolytes, aqueous ones are more attractive for practical use, which reduces the difficulty of capsulation and the contamination. Bach et al. developed an aqueous electrolytes containing ferricyanide $[Fe(CN)_6^{4-/3-}]$ redox couple. After optimization, a PCE of 4.1% was achieved using Pt CE.[23c] This result undoubtedly strides forward to a greener and cheaper aqueous DSCs system.

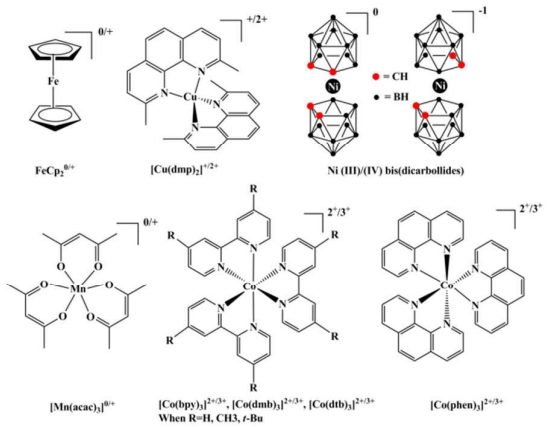

Fig. 6 Molecular structure of Fe, Ni, Cu, Mn, and Co complexes.

Fukuzumi et al. applied Cu complexes of $[Cu(SP)(mmt)]^{-/0}$, $[Cu(dmp)_2]^{+/2+}$, $[Cu(phen)_2]^{+/2+}$ as the redox couples for DSCs.[24a] Based on Pt CE and N719 dye, the DSCs employing $[Cu(SP)(mmt)]^{-/0}$, $[Cu(dmp)_2]^{+/2+}$, $[Cu(phen)_2]^{+/2+}$ redox couples obtained PCE values of 1.3%, 1.4%, and 0.1% respectively. The low performance can be attributed to the mismatching between the energy level of the applied sensitizer and the copper complex redox couples. Wang group introduced an organic dyes named C218 into the redox couple of $[Cu(dmp)_2]^{+/2+}$ in DSCs.[24b] With conductive Cb deposited Pt as CE, a high PCE of 7.0% with high V_{oc} of 0.932 V was achieved. Interestingly, they found that the redox couple exhibited very lower electron transfer rates on some noble metals, Cb, or conducting oxides, generating a poor FF. Thus, it is urgent to develop an effective CE catalyst to improve the performance of the DSCs using this copper redox couple.

Hupp et al developed Ni complexes ($Ni^{3+/4+}$) as the redox couples in DSCs.[25a] Among the Pt, Au, and Ag CEs, and they found that the DSCs using Au CE showed the highest J_{sc}, FF, and PCE (1.5%), owning to the better electrode reflectivity, increasing the utilization of the illumination. Further, they compared a class of $Ni^{3+/4+}$ redox couples by changing the ligands and the researchers can obtained more information about the tuned redox potential, shuttle polarity, solubility, and binding properties. The devices using this kind of $Ni^{3+/4+}$ CEs gave PCE values of 0.7~2.0%.[25b] Oyaizu et al. introduced oxovanadium(IV/V) redox couple into DSCs. With Pt CE, the device showed a PCE of 5.4%.[26] Spiccia et al. used manganese (Mn) complexes of $[Mn(acac)_3]^{0/+}$ as redox couples for DSCs.[27] They found that PEDOT CE behaved better than Pt and Au,

combined with the $[Mn(acac)_3]^{0/+}$ and a new sensitizer named K4. When applied the commercially available MK2 or N719 sensitizers, the device showed a PCE of 4.4% with the help of PEDOT CE.

Compared to the aforementioned redox couples, Co complex, have lower extinction coefficients in the visible light region, diminishing the competition with photosensitizers. And Co redox couple is the widely studied metal complex by changing the ligands, resulting in different redox potentials, solubility, stability, absorbance, etc. With regard to Co complex redox couples, different kinds of CE catalysts have been applied to catalyze the regeneration. Pt is also the most commonly used CE catalyst thanks to its superior conductivity and catalytic activity towards Co redox couples regeneration. Using $Co^{2+/3+}(bpy)_3$ as electrolyte, Grätzel group have obtained a DSCs with a PCE of 12.3% among various Co redox couples using Pt CE and co-sensitizers of zinc porphyrin (YD2-o-C8) and organic dyes (Y123).[28] This result suggests that Pt can effectively catalyze the reduction of Co^{3+} to Co^{2+}. Although Co based redox couples have many advantages, the charge recombination between them and dye are great. Boschloo's research revealed that the recombination can be prevented by choosing an appropriate sensitizer such as organic dye composed of donor-π-accepter bridge.[29] Although Pt has excellent catalytic activity toward Co redox couple, it is an expensive and scare noble metal. Thus finding ~~low-cost~~ Pt-free catalysts to replace Pt is also urgent to decrease the cost and to improve the competitiveness of Co redox couple based DSCs. Previous research proved that glassy carbon showed better reversible cyclic voltammograms towards Co complex redox couple than Pt,[30] indicating a more reversible electron transfer on glassy carbon. Hence carbon should be a potential candidate for Pt in Co complex system.

Ca and ordered mesoporous carbon (OMC) were carried out to catalyze Co complex.[31] EIS exhibited much smaller R_{ct} for Ca and OMC than Pt in catalysing the reduction of Co^{3+} to Co^{2+}, corresponding to higher PCE values of Ca (3.43%) and OMC (4.05%) than Pt (2.91%) in DSCs system. Boujtita et al. prepared a screen printed carbon electrodes (SPCEs).[32] Although the J-V characterization of SPCE/Co redox couple cell was 30% lower than that of Pt/Iodide redox couple cell both without optimization, the screen printing process was a reproducible manufacturing for a stable and conductive carbon film, which was suitable for industrialization. Considering the portable applications, flexible plastic CE has been fabricated by deposited SWCNTs on plain polyethylene terephthalate (PET) substrates.[33] The R_{ct} of SWCNT was 0.6 Ω m^2, much smaller than Pt on ITO-PET (4 Ω cm^2) and Pt on FTO glass (1.7 Ω cm^2). However, the R_s of SWCNT/PET without ITO layer was larger than the two kinds of Pt CEs. Thus the SWCNT/PET CE displayed similar performance to Pt/ITO-PET or FTO glass for Co redox couple based electrolyte. Moreover, graphite and Cb were also tested as CE catalysts for Co^{3+} reduction, which performed equivalent to that of Pt.[34]

Many carbon catalysts were applied for Co redox couple and were initially worked well, but were unstable.[30] Graphene nanoplatelet (GNP) was found to have superior electrocatalytic activity towards Co redox couple with better stability under potential cycling than that of Pt.[35] The test of photo-to-electron property witnessed that the PCE exceeding 9% for GNP CE outperformed that of 8% for Pt CE under comparable conditions. Studies revealed that the active sites for charge transfer on GNP/electrolyte interface were defects and oxidic surface groups on GNP, which can be illustrated by the fact of that optical absorbance of GNP electrode was inversely proportional to R_{ct} value.[35a] This means that more mass loading of GNP leads to smaller R_{ct} and better catalytic activity. However, for a given transparency, the R_{ct} for GNP/$Co^{2+/3+}$ was 60 or 300 times smaller than that for Pt/I^-/I_3^-. Such excellent electrochemical catalytic activity of graphene enables GNP/$Co^{2+/3+}$ based DSCs can maintain high photovoltaic performance with semi-transparent GNP CE. Whereas, the splendid catalytic activity of GNP for $Co^{2+/3+}$ cannot be extended to other redox couples such as I^-/I_3^-. Aksay group introduced functionalized graphene sheet (FGS) as CE by using ethyl cellulose as sacrificial binder which was partially pyrolyzed.[36] The prepared FGS had large surface area containing lattice defects and oxidic functional group of hydroxyls, epoxides, and carboxylic acids, which were essential for a promising catalyst. Moreover, the binder residue can improve the electrode's structural stability in acetonitrile containing electrolyte. Importantly, the prepared FGS electrodes were versatile and performed as well as or even better than Pt CEs for I-, Co-, and S- based redox couples.

Since the GNP CE was mechanically unstable due to the poor adhesion between GNP and substrate, GNP detaching from the supporter may be responsible for the high dark current for GNP based DSCs. Many researches were focused on improving the mechanical stability of graphene CE through increasing adhesion to the supports. Graphene oxide (GO) is an amphiphilic graphene material which derives from the abundant oxidic functional groups on the condensed aromatic backbones. Kavan's group fabricated GO film with wear resistance and good adhesion to FTO substrate, which was claimed probably caused by intimated interaction of the hydrophilic groups in GO and the hydroxylated surface on FTO surface.[37] They found that pristine GO CE showed almost no activity towards reducing Co^{3+}, indicating the sole presence of oxidic functional groups on carbonaceous skeleton was not essential for catalytic activity. When the GO film was reduced through hydrazine or heat treatment, the electrocatalytic activity was improved dramatically. In view of this phenomenon, they presumed the activity to be stemmed from the dangling bonds at the graphene edges. DSCs with thermally treated composite of GO and GNP as CE exhibited the best photovoltaic performance exceeding 9%.

Furthermore, doping or loading was an efficient method employed for graphene nanoplatelets to improve catalytic activity and mechanical stability of graphene CE. TaON nanoparticles embedded in reduced GO nanocomposites (TaON-RGO, Fig. 7a) were prepared by Wang et al.[38] The composite possessed much better catalytic property towards $Co^{2+/3+}$ than sole RGO or TaON, suggesting the synergistic effect from intimate interaction of RGO and TaON. Silver

nanowires (AgNWs) are promising nanomaterial for energy application owing to their unique electrical and optical properties. Kim et al. prepared hybrid AgNW/GNP as CEs for the reduction of Co^{3+}, obtaining a PCE higher than individual GNP or AgNW CEs similar to that of Pt CE.[39] In addition, heteroatom-containing graphene was also synthesized served as CEs in DSCs system for Co redox couples. Both carbon and nitrogen doped graphene can enhance mechanical stability as well as maintain catalytic performance. The resulting PCEs were all better than Pt.[40]

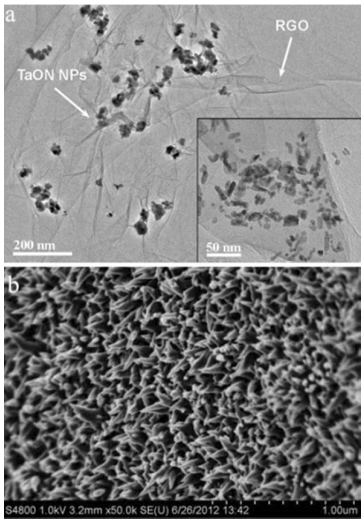

Fig. 7 (a) TEM image of TaON/Pt composite;[38] (b) SEM image of PANI nanowires.[45]

A wide variety of transition metal compounds with outstanding electrochemical property opens a new horizon for Pt-free CEs based on inorganic materials. TiC and NbO_2 have been introduced into Co mediated DSCs.[31] The EIS measurements showed that the TiC and NbO_2 owned much smaller R_{ct} towards the reduction of Co^{3+} than Pt, corresponding to higher PCE for TiC and NbO_2 based DSCs. Moreover, a pyrite (FeS_2) film was prepared as CE for Co mediated DSCs, and a PCE of 6.34% was achieved. It was found that the charming catalytic activity of FeS_2 was attributed to the good optical reflectivity, which enhanced the light distribution in the cell as a result of improving current.[41] In addition, the nanocomposites of cobalt selenide and nickel selenide ($Co_{0.85}Se/Ni_{0.85}Se$) were prepared and used as CEs, which manifested better catalytic activity for Co redox electrolyte than Pt.[42] However, the poor adhesion of transition metal compounds to FTO glasses and the requirement of a large quantity of compounds load for high efficiency still limited the application of these materials.

Among various Pt-free CE catalysts, conductive polymers play an important role because of their high conductivity, good plasticity, low cost, and high catalytic activity as well. PEDOT was found an outstanding conducting polymer utilized as CE for Co^{3+} reduction.[43] Grätzel group fabricated a DSCs using PEDOT CE in conjunction with Co redox couple, yielding an excellent PCE of 10.3%.[43a] The result of the current transient test announced the absence of photocurrent decay for PEDOT, indexing an alleviated diffusion limitation of Co reduction current, which may help maintaining the maximum of the attainable current in the cell. They suggested this effect to be due to the 3-dimensional and porous morphology of the PEDOT layer, which reduced the diffusion distance and generated diffusion fields with radial symmetry. Carli et al. compared three different kinds of PEDOT based CEs with different additives, including $LiClO_4$ (ClO_4), sodium dodecylsulfate (SDS), and polystyrenesulfonate (PSS). The PEDOT/ClO_4 electrodes were found to be the best performance among the three CEs towards the Co redox couple.[43b]

Apart from PEDOT, some other organic materials were also attempted to act as CE catalysts for Co redox couples. The most challenging one was nanoporous poly(3,4-propylenedioxythiophene) (PProDOT) introduced by Yum et al. With a large surface area, PProDOT owned much lower R_{ct} (2.5 Ω) in comparison to that of 50 Ω for Pt, leading to an advanced FF and a higher PCE of 10.08% for Co mediated DSCs.[44] PANI was another fairly good alternative for Co^{3+} reduction due to its good catalytic activity and simply fabrication process in low temperature. Compared to drop-cast PANI film with random network, an oriented PANI nanowires array (Fig. 7b) were grown in situ by Wang et al., along which structure the electron transfer was expected to be faster.[45] The R_s and R_{ct} of PANI nanowires array were smaller than those of drop-cast PANI film as expected; hence a better photovoltaic performance of 8.24% was observed.

Organic conducting polymers are promising candidates for CE catalysts, which are most likely to realize plastic applications on account of their simply low temperature fabrication process. The experimental conditions and results about the metal complex redox couples based DSCs using different counter electrode catalysts are summarized in Table S6.

2.4 CE catalysts for hole transport materials (HTM)

Although recent studies on liquid electrolyte based solar cells have raised the highest PCE to 13% after successive advances in sensitizers and electrolytes, there is debate over whether a liquid electrolyte may limit the realization of stable and efficient DSCs for commercial applications. To overcome these disadvantages, alternative liquid-free electrolytes have been a long-term goal in this field.[2c] As a consequence, solid state DSCs (ssDSCs) have been extensively studied for their advantages in avoiding leakage and corrosion. Similar to conventional liquid DSCs, the basic configuration of ssDSCs includes a conducting glass substrate (FTO or ITO), a mesoporous TiO_2 film anchored with dye molecules, a CE, and hole transport materials (HTM) to replace the liquid redox electrolyte.[46] The HTM for ssDSCs must be able to transfer holes from the oxidized state dye. The CE mainly collects the charges to complete an electronic circuit. In ssDSCs, the CE should have high conductivity, mechanical stability and chemical/electrochemical stability. Moreover, to match the HTM, a CE with a large work function is also required.

Currently, most HTM based ssDSCs use a noble metal layer (such as Pt, Au, or Ag) for the hole collecting CE.

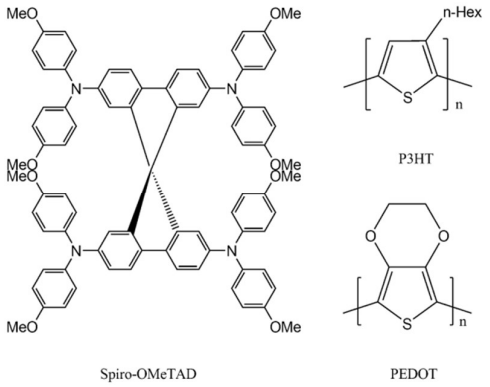

Fig. 8 Schematic diagram of the HTM of Spiro-OMeTAD, P3HT, and PEDOT.

Although most studies are focused on inorganic[47] or organic small molecule HTMs,[48] the CE is still a key component in ssDSCs. In 1998, using Pt as a CE, Grätzel et al. reported efficient ssDSCs using N_3 dye and amorphous 2,2′,7,7′-tetrakis-(*N,N*-p-methoxyphenyl-amine)-9,9′-spirobifluorene (sprio-OMeTAD, Fig. 8) as HTM, with which a maximum IPCE of 33% and an overall PCE of 0.74% were obtained.[49] The low PCE was caused by interfacial recombination losses. This system was further optimized in 2011 using a cobalt complex as a dopant, employing a high absorption coefficient organic dye (Y123) and thermally evaporating 200 nm of Ag CE, whereby the PCE of spiro-OMeTAD based ssDSCs was improved to 7.2%.[50] Thus far, spiro-OMeTAD remains the most effective organic HTM for ssDSCs. However, previous studies have demonstrated that spiro-OMeTAD still faces serious challenges such as a high synthetic cost and low hole mobility.[51] In parallel with spiro-OMeTAD, several other molecular and polymeric p-type organic semiconductors such as PANI,[52a] PPy,[52b] poly (3-hexylthiophene) (P3HT),[52c] and PEDOT[52d] have been successfully implemented in HTM based ssDSCs. Recently, an inorganic perovskite, $CsSnI_3$, was reported as an efficient HTM in ssDSCs. After optimization, the PCE of ssDSCs with the inorganic semiconductor $CsSnI_{2.95}F_{0.05}$doped with SnF_2 as an HTM, N719 dye and a Pt CE improved to 10.2% under standard AM 1.5, which was the highest efficiency of ssDSCs obtained by utilizing an inorganic HTM to date.[53] Generally, the PCE of ssDSCs still cannot compete with that of liquid DSCs. In the pursuit of significantly increasing the performance of ssDSCs, the interfacial contact between the HTM and the photoanode or CE should be of serious concern, as it plays a key role in improving the hole or electron collection, and hence the PCE.

In 1995, a ssDSCs with CuI as an HTM was reported, using evaporation of Au film as the CE to realize electrical contact.[47a] The PCE of CuI based ssDSCs has subsequently been greatly increased to 3.75% by the addition of the CuI crystal growth inhibitor triethylamine hydrothiocyanate (HTT) and the use of Au film as the CE.[54] CuI as an HTM still poses some challenges, including a detectable drop in J_{sc} and V_{oc} when the cell is illuminated for several hours. However, with the evaporation of 30 nm of Au CE, a record efficiency of 4.1% for ssDSCs was attained using the dye D102 and sprio-OMeTAD as the HTM.[55a] To effectively fill thick nanoparticle based mesoporous TiO_2 films with HTM, the Gao group fabricated high efficiency ssDSCs using multilayer TiO_2 coated ZnO nanowire arrays sensitized with Z907 dye as the photoanodes and developed a multi-step sprio-OMeTAD HTM filling process that effectively fills sensitized films as thick as 50μm with HTM, in which a 100 nm thick layer of Au was deposited by e-beam evaporation on top of the HTM as the CE. The resulting ssDSCs yielded an average PCE of 5.65%.[55b] At the same time, polymer HTM penetration into the TiO_2 porous electrodes has been accomplished via the in situ polymerization of pre-penetrated monomers. For example, Liu et al. reported an indoline dye (D149) based DSC with in situ photoelectron-polymerization of bis-EDOT forming the polymer HTM. Using Au as the CE, the devices give an average PCE of 6.1%, representing a remarkable improvement for polymer HTM-based ssDSCs.[56]

As with liquid DSCs, Pt film is a conventional CE in ssDSCs. The Liu group fabricated flexible ssDSCs on ~~low cost~~ Ti foil substrate using D102 as the sensitizer, P3HT as the HTM, and a semi-transparent Pt CE. Because Ti substrate is non-transparent, the device must be illuminated from the rear side, by which a significant proportion of the radiation is absorbed and scattered by P3HT and Pt, respectively. It is therefore important to limit the amount of Pt and P3HT to reduce absorption and scattering. Under optimized conditions, a PCE of 1.20% is obtained for the devices illuminated from the Pt CE side. The lower efficiency compared to conventional devices is due to light loss from the Pt CE and strong absorbance from the P3HT layer.[57] In addition, Pt CE is usually used in sandwich-type ssDSCs. The Kim group reported an in situ solid state polymerizable method for the preparation of PEDOT HTM based ssDSCs with an excellent performance and improved electrode/HTM interfacial properties using N719 dye and a Pt CE.[58] The device gave a PCE of 5.4%.

Although Ag CE is not suitable for liquid iodide electrolyte based DSCs because it is easily dissolved by iodide electrolytes, Ag is a common CE in ssDSCs. Ag CE can be fabricated via a thermal evaporation method[59] or by spray solution containing Ag nanoparticles on top of the device.[60] All of these electrodes require an annealing step to optimize the conductivity, which process causes rapid ssDSCs degradation. It is therefore of great interest to find a method for fabricating Ag film with low sheet resistances and high transmission without annealing. The McGehee group fabricated Ag nanowire (Ag NWs, Fig. 9a) mesh on a separate substrate and then transferred it using proper pressure on the top of sprio-OMeTAD, thereby achieving comparable device performance with standard thermally deposited Ag electrodes.[61] The laminated Ag NWs are limited due to the pressing procedure, whereby each wire may come into contact with the soft hole conductor to be transferred, and are too thick to be completely transferred to another substrate. A new process, completely in solution, was then developed for Ag NW/PEDOT: PSS composite electrodes at room temperature, and the device showed a PCE of 3.7%.[62]

Obviously, the fact that these CEs use high cost metals is still an issue for HTM based ssDSCs in wide scale applications. Carbon, on the other hand, is an abundantly available and low cost material that can be deposited through a simple process such as screen printing or spray coating. Cb and graphite are the most common carbon materials that have been used in ssDSCs.

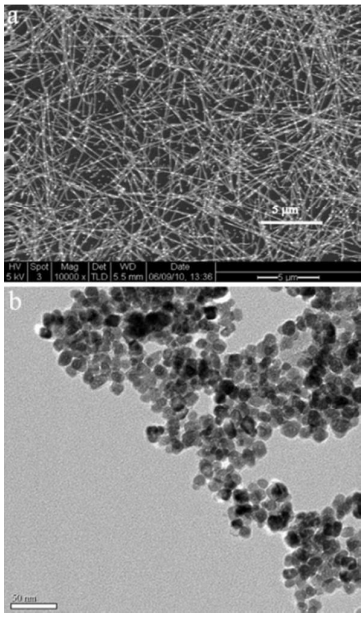

Fig. 9 (a) SEM image of Ag NWs;[61] (b) TEM image of ITO nanoparticles.[69]

In 2002, the O'Regan group reported ssDSCs using CuSCN as HTM, TiO_2 as the electron conductor, N3 dye and graphite as the CE. The device showed a J_{sc} of 8 mA/cm^2, V_{oc} of 600 mV, and PCE of 2% at 1 sun, similar to the results of CuSCN based ssDSCs with an evaporated Au CE.[63] The Sakamoto group prepared large surface area CEs blending nano size Cb in the PEDOT: PSS dispersion, after which the CE with the larger number of NCS groups was covered with a solution containing guanidine thiocyanate. The resulting ssDSCs exhibited a dramatically higher PCE of 7.4%. The EIS results revealed that adding nano-size carbon decreased the CE/HTM interface resistance, while the lower electrical resistance of PEDOT: PSS with carbon also contributed to the higher cell performance.[64] The Han group have developed highly efficient P3HT based ssDSCs with low cost carbon CEs. Compared to blank graphite CE based devices, those with graphite and Cb CEs show a PCE of 3.1%. The EIS results further indicated that Cb enhanced electron injection from the CE to P3HT, leading to a decreased recombination rate between injected electrons and holes.[65] Recently, the same group further optimized the ratio of Cb in the graphite CE, whereby a considerable efficiency of 4.03% was obtained combined with spiro-OMeTAD and the organic dye D102.[66]

To broaden the selected scope of electrode materials in ssDSCs, metal oxides have been studied because those with high work functions satisfy certain basic requirements for CEs in ssDSCs. In 2010, the Xia group used V_2O_5/Al as a novel CE in ssDSCs with spiro-OMeTAD as the HTM.[67] They observed that the performance of these ssDSCs depended on the thickness of the V_2O_5 film. If it is too thin to cover the sprio-OMeTAD layer, it can cause a short-circuit, whereas if the film is too thick, it can result in bad conductivity. The ssDSCs with a 10 nm thick V_2O_5/Al CE reached a PCE of 2.0% after optimization, approaching the performance of ssDSCs using Ag CE. The Chen group reported bifacial transparent ssDSCs based on an indium tin oxide (ITO)/Au CE made through sputtering technology and obtained an efficiency of 1.96% through photoanode side illumination and 1.50% through ITO CE side illumination.[68] In the pursuit of non-sputtered and non-noble metal CEs, the Han group recently reported a fully printable transparent ssDSCs with a mesoscopic ITO CE. Fig. 9b is the TEM image of the ITO nanoparticles.[69] The ssDSCs with D102 dye and spiro-OMeTAD HTM presented a PCE of 1.73% when irradiated from the front side and 1.06% when irradiated from the rear side. The experimental conditions and results of the hole transport material (HTM) based DSCs using different counter electrode catalysts are summarized in Table S7.

Fabricating highly efficient and low cost ssDSCs is one major challenge in this area. Most studies currently focus on developing small organic molecule HTMs and add various dopants to improve the conductivity of the HTM and its pore-filling property. However, studies on non-metal CEs in ssDSCs are also important to improve the fabrication process and to reduce the cost of the ssDSCs.

3. Counter electrode in quantum dots-sensitized solar cells (QDSCs)

Quantum dots (QDs) is an attractive photo-absorber because of the advantages of large absorption coefficients and tunable absorption onset in the visible region by regulating the particle size and composition. Based on the DSCs' structure, QD is introduced into DSCs as an alternative to the dye, and the produced devices are called QDs-sensitized solar cells (QDSCs).[70] Although the redox couples in DSCs can be transferred into QSCs system, the S^{2-}/S_n^{2-} (polysulfide) redox couple has proven the most effective one so far because of its optimal redox potential, efficient hole extraction from the QDs, and ability to chemically stabilize QDs such as CdS, PbS, and Ag_2S. The CE catalysts must be able to recycle the electrolyte to complete the circuit. The common CE catalyst used for evaluating QDSCs is Pt and Au. However, the noble metals are quickly poisoned by the polysulfide electrolyte, resulting in significant drops in current. Thus, the Pt and Au CE are unsuitable for long term use in QDSCs. Moreover, Pt and Au are rare and expensive, and replace them with an inexpensive, earth-abundant material is an ideal solution.

The metal sulfides such as Cu_2S, PbS, and CoS are highly active in polysulfide reduction, although early studies have shown that they may be not stable under normal operating conditions. Specifically, the PbS device dropped to 10% of its initial current density after two weeks.[71] Consequently,

choosing a suitable CE catalyst is important to create highly efficient and stable QDSCs. In this section, we will discuss the various CE catalysts, including metals, metal sulfides, carbides, nitrides, carbon materials, polymers, and multiple compounds, and note the advantages and disadvantages of each.

Although Pt and Au are not the best choice for CE catalysts in QDSCs due to the poison effect, there are a few reports on them. Choi et al. synthesized AuPt bimetallic nanoparticles (AuPt-BNPs) with a dry plasma reduction (DPR) technique and introduced them in QDSCs as a transparent CE which exhibited a high catalytic activity. The device employing the AuPt-BNP CE reached a PCE of 2.4% under front side illumination and 2.2% under rear side illumination.[72a] Although the performance of AuPt-BNPs is higher than both Pt and Au CEs, they are still not the ideal CE for QDSCs. In the polysulfide redox couple system, sulfur atoms are adsorbed on the Pt surface, suppressing the surface activity and conductivity. To overcome this issue, a thin passivating layer of CuS was deposited on the Pt surface to prevent the corrosion from the polysulfide redox couple. The QDSCs with a CuS-modified Pt CE gave a PCE of 2.27%, much higher than Pt based QDSCs.[72b] Another solution is to replace the S^{2-}/S_x^{2-} redox couple with a non-corrosive redox electrolyte. Sun et al. introduced the organic redox couple of TMTU/$TMFDS^{2+}$ (Fig. 5).[72c] This device produced a PCE of 0.86% with a high FF of 0.58 due to the reduced impedance between the electrolyte and the Pt CE. The performance of the TMTU/$TMFDS^{2+}$ based device reached an efficiency three times higher than that of the device based on common S^{2-}/S_x^{2-} electrolyte (0.27%). They also applied another organic redox couple, $McMT^{-}$/BMT.[72d] Combined with a Pt CE, the device yielded a PCE of 0.6%, much higher than the conventional S^{2-}/S_x^{2-} redox couple based device (0.3%). The EIS results showed that the charge recombination in the $McMT^{-}$/BMT based QDSCs was much lower than that in the polysulfide based QDSCs. In addition to the organic redox couple, metal complex redox couples were also tested. Morris et al. compared $Mn^{2+/3+}$ and $Co^{2+/3+}$ complexes as promising redox couple alternatives in QDSCs.[72e] High V_{oc} values of approximately 1 V were achieved in a liquid-junction solar cell (a three-electrode arrangement employing a quantum dot-sensitized photoanode as the working electrode, a Pt CE, and a Ag/AgCl reference electrode). The low solubility of the $Mn^{2+/3+}$ electrolyte prevented the redox mediators from sustaining high photocurrent due to mass transport limits. Although the FF was up to 0.6, a low PCE of 0.33% was achieved under 0.2 Sun. Compared to $Co^{2+/3+}$, $Mn^{2+/3+}$ showed more positive reduction potentials and slower recombination rates. Improving solubility is one of the key issues for metal complex redox couples in QDSC systems.

The most commonly used CE materials are metal sulfides, among which copper sulfides are the most widely used because of their superior catalytic activity toward polysulfide electrolyte redox couples.[73] Specifically, Cu_2S deposited on brass foil is the most commonly used CE in high efficiency QDSCs. However, the corrosion caused by polysulfide poses an obstacle for the brass substrate. To resolve this problem, the brass substrate is commonly replaced by FTO glass. Zhong et al. deposited a Cu_2S film on FTO glass by electrodeposition of a copper film via a multipotential step technique followed by dipping it into polysulfide methanol solution. As shown in Fig. 10a, the Cu_2S film takes on an interconnected nanoflake shape.[74a] A CdSe based device with an optimized Cu_2S/FTO CE exhibited a PCE of 5.21%, comparable to that of the commonly used Cu_2S/brass CE (5.41%), while the Cu_2S/FTO CE showed good stability at the working conditions over 10 h, showing no decrease in PCE, which was a severe challenge for the Cu_2S/brass CE.

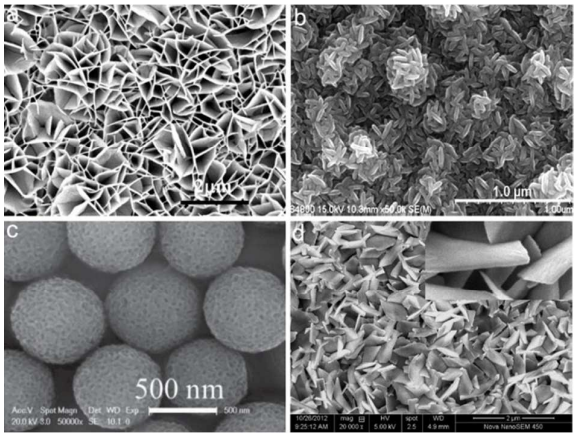

Fig. 10 SEM images of sulfide catalysts: (a) Cu_2S;[74a] (b) NiS;[77a] (c) m-Fe2S;[78a] (d) Bi2S3.[79b]

The Zhao group prepared CuS nanosheet film on FTO glass with a facile and low temperature hydrothermal method to prepare CEs for QDSCs.[74b] The thickness of the CuS film was controlled by the precursor Cu film with thicknesses of 0.1, 0.2, 0.5, 1.0, and 2.0 μm. Under front side illumination, the QDSCs using the CuS CE prepared with 1.0 μm Cu yielded the highest PCE of 3.65%. Most importantly, all CuS CEs behaved better than Pt CE. Interestingly, a thinner CuS CE prepared with a ~0.2 μm thick Cu film showed excellent transparency. A bifacial QDSC was achieved using this transparent CE, and a similar PCE was achieved under both front and rear illumination. Wang et al. prepared a Cu_2S CE by ion exchange of ZnS films deposited on mesoporous ITO electrodes with a Cu^{+} containing electrolyte solution. This device with Cu_2S CE exhibited a high PCE of 4.78%, matching the performance of a Cu_2S/brass-based device. The ion exchange technique is a promising route to fabricate other sulfide CEs, such as PbS, CoS, etc.[74c] Meng used a mesh structured Cu_2S CE in tandem QDSCs which produced a PCE of 3.65%.[74d] A Cu_2S nanorod CE was also applied and a PCE of 4.12% was achieved.[74e] The Lee group synthesized $Cu_{1.8}S$ microspheres with a diameter of 500 nm as CE catalysts and the device produced a PCE of 3.65%.[75a] Koo et al. developed a simple hydrothermal method to synthesize a $Cu_{1.8}S$/CuS film on FTO glass as an efficient CE for QDSCs.[75b] Under the illumination of one sun (100 mW cm^{-2}), a device using the prepared $Cu_{1.8}S$/CuS CE gave a PCE of 1.66% with J_{sc}=5.46 mA cm^{-2}, V_{oc} = 0.539 V, and FF= 0.564. A compact (c-Cu_xS) and a porous (p-Cu_xS) film on FTO glass were obtained

through a chemical bath deposition (CBD) technique and used as CEs in QDSCs.[75c] Compared to the c-Cu_xS film, the p-Cu_xS film exhibited an enhanced catalytic activity and the QDSCs yielded a PCE of 3.17%. The number of redox active reaction sites in the p-Cu_xS film is 57.9% higher than those available in the c-Cu_xS film, resulting in the improved performance of p-Cu_xS CE based QDSCs.

The Zaban group prepared a PbS CE on Pb metal, and the device yielded a PCE of 3.01%, much higher than the Pt CE based device (0.8%).[76a] EIS reveal that the high performance of the PbS CE is the result of the improved charge transfer at the CE/electrolyte interface, causing a change in the ion concentration in the solution by reducing the recombination rates at the working electrode/electrolyte interface and strongly impacting both the J_{sc} and the FF. Kim et al. studied the impact of Mn^{2+} doping on the catalytic activity of PbS CEs.[76b] The QDSCs with a Mn^{2+} doped PbS CE showed a PCE of 3.61%, which was ~40% higher than that of the device with the bare PbS CE (2.59%). The catalytic ability of the PbS CE was improved significantly by Mn^{2+} doping, which can be attributed to the following two reasons: intentional impurities impact the structure of the host material, increasing the surface roughness, and the Mn^{2+} dopant creates new energy states which can delay the exciton recombination time and allow charge separation to be activated. Interestingly, Mn^{2+} doped PbS QDs also behave as additional photoelectron donors under illumination, resulting in vigorous redox reactions in the polysulfide electrolyte. The Gopi group prepared NiS CE with a facile and low temperature CBD method under different temperatures of 80, 90, and 100 °C.[77] The NiS (Fig. 10c) CE prepared at 90 °C showed the highest catalytic activity toward the polysulfide redox couple, and the device gave a PCE of 3.30%, higher than the Pt CE based device (1.89%). Ion sulfides have also been used as CEs in QDSCs.[78] Mesoporous honeycomb-like FeS_2 microspheres (m-FeS_2, Fig. 10c) with diameters of 500~800 nm and pore sizes of 25-30 nm along with solid FeS_2 microspheres (s-FeS_2) with diameters of approximately 2 μm have been synthesized with a simple solvothermal method.[78a] Both types of FeS_2 microspheres present more effective catalytic activity in QDSCs than Pt, while the m-FeS_2 behaved better than s-FeS_2. As a consequence, using a ZnO/ZnSe/CdSe photoanode, the QDSCs with m-FeS_2 CE yielded a PCE of 3.90%, higher than the performance of the s-FeS_2 CE based device (3.50%). Liu and Li et al. prepared FeS and FeS/Fe_3S_4/Fe_2S CEs on carbon steel substrate. The FeS device produced a PCE of 3.34% with a high J_{sc} of 20.40 mA cm^{-2}, much higher than the FeS/Fe_3S_4/Fe_2S CE based device (1.76%).[78b,c] MoS_2, Bi_2S_3 (Fig. 10d), and CoS have also been used as CEs in QDSCs, presenting decent catalytic activity.[79a-c] With the SILAR method, Li deposited CuS, CoS, NiS, and PbS on ITO porous films for use as CEs in QDSCs.[79d] They found that CuS CEs with 12 SILAR cycles exhibited the highest catalytic activity, followed by the CoS CE, and that NiS and PbS CEs showed similar catalytic activity, significantly lower than that of a Pt CE.

We fabricated ~~low-cost~~ QDSCs based on the earth abundant element SnS quantum dot with S^{2-}/S_x^{2-}, T^-/T_2, and I^-/I_3^- redox couples, comparing the performance of CE catalysts of Pt, TiC and SnS.[80a] The results indicated that Pt and TiC showed similar catalytic selectivity toward I^-/I_3^- and SnS was not an ideal catalyst for I^-/I_3^-. However, TiC behaved better than Pt for T^-/T_2. With a TiC CE and T^-/T_2 redox couple, the SnS based QDSCs yielded a PCE of 1.03%, much higher than the device using the S^{2-}/S_x^{2-} redox couple (0.16%). These results indicate the great potential of transition metal carbide catalysts in organic redox couple based QDSCs. In addition to TiC, TiN was also applied in QDSCs as a CE, which produced an unsatisfactory PCE of 0.8%.[80b] Loading the TiN on graphene or CNTs may greatly improve the catalytic activity.

As in DSCs, carbon materials are also competitive CEs for QDSCs. In 2010, an ordered multimodal porous carbon (OMPC, Fig. 11a) was developed as a CE for QDSCs. The corresponding QDSCs employing the OMPC CE present a PCE of 4.36%, significantly higher than those of Pt and Ca CE based devices (2.29%, Pt and 3.30%, Ca).[81a] The unique mesoporous structure endows the OMPC with a large surface area and a well developed 3D interconnected ordered macropore framework with open mesopores embedded in the macropore walls. This allows the electrode to have fast mass transfer kinetics toward the polysulfide electrolytes, which is the major reason behind the high catalytic activity of OMPC over Ca and Pt. Yu et al. compared hollow core mesoporous shell carbon (HCMSC) with Pt in QDSCs using I^-/I_3^- and polysulfide redox couples.[81b] For the expensive Pt CE, the S^{2-}/S_x^{2-} redox couple showed better matching ability than the I^-/I_3^- redox couple, and the QDSCs using S^{2-}/S_x^{2-} and the Pt CE gave a PCE of 1.05%. The S^{2-}/S_x^{2-} based device using an HCMSC CE demonstrated a PCE of 1.08%, much higher than devices using mesoporous carbon, CMK. The higher catalytic activity of HCMSC can be attributed to its unique structural characteristics, such as large specific surface area, high mesoporous volume, and a 3D interconnected well-developed hierarchical porosity network, all of which facilitate fast mass transfer with less resistance of the polysulfide electrolyte.

Lee et al. prepared a mesocellular carbon foam with a high surface area of 911 m^2 g^{-1} and a large pore size of 25 nm. The CdS/CdSe/TiO_2 QDSCs using this carbon foam CE show a PCE of 1.75%, much higher than those of the devices employing Pt CE (1.22%) or carbon CE (0.94%).[81c] The large surface area of the carbon foam provides more effective catalytic sites for S_x^{2-} reduction while the ~25 nm mesochannels with an interconnected pore structure facilitate electrolyte diffusion. As a result, the carbon foam CE shows much improved catalytic activity in comparison to the conventional Pt and carbon CEs. Furthermore, they introduced the carbon foam CE to a ZnO nanowire array photoelectrode based QDSCs.[81d] The cell with the carbon foam CE yielded a higher PCE of 3.60%, which was much higher than that of the TiO_2 photoanode based QDSCs, because the ZnO nanowire structure provided efficient photoelectron collection and light harvesting. Similarly, the carbon foam CE exhibits a low R_{ct} between the CE/electrolyte interface due to the extremely high surface area and facile diffusion of the redox couple compared to conventional Pt and Au CEs. Furthermore, the carbon foam

electrode is much more durable in the polysulfide electrolyte than Au and Pt electrodes. Carbon nanofiber (CNF) has been used as a CE in SnO_2 photoanode based QDSCs.[81e] The device using CNF CE showed a PCE of 2.5%, surpassing the Pt CE based device (2.1%). Zhu et al. inspected the impact of N-doping on the performance of hollow carbon nanoparticle (HCNP) CEs in QDSC systems. The QDSCs using this N-doped carbon CE achieved a PCE of 2.67%, higher than HCNP, CNTs and Pt CE based devices. The EIS results revealed that the R_{ct} of the N-HCNP CE toward the polysulfide redox couple greatly decreased compared to that of HCNP, CNT and Pt CEs. In addition, the N-HCNP electrode showed better electrochemical stability and tolerance to sulfur poisoning in the polysulfide electrolyte. The better performance of the N-HCNP electrode is primarily attributed to the fact that N-doping may introduce more active catalytic sites in the porous structure, although this conclusion needs further validation.

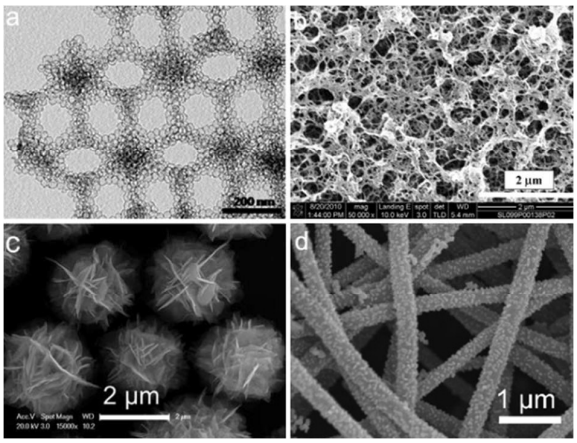

Fig. 11 (a) TEM image of OMPC;[81a] SEM images of (b) PEDOT;[82a] (c) $CuSnS_3$;[75a] (d)CuS/Cf.[85b]

Ho et al. introduced conducting polymers of polythiophene (PT), PPy, and PEDOT (Fig. 11b) as CEs into QDSCs.[82a] The QDSCs with a PEDOT CE exhibited the highest PCE of 1.35%, much higher than those of the devices using Pt CE (0.09%) or PPy CE (0.41%). EIS results showed that the PEDOT CE had higher electrocatalytic activity and lower R_{ct} at the CE/electrolyte interface than either PT or PPy. The SEM images depicted a regular porous structure in PEDOT with net-like fibers of various dimensions, while the others did not exhibit any special matrix structure, explaining why PEDOT possesses the highest catalytic activity toward the polysulfide redox couple among the three polymers. Shu et al. compared different CE catalysts with the organic redox couples of T^-/T_2 and $C_7H_5N_4S^-/C_{14}H_{10}N_8S_2$ (AT^-/BAT) in QDSC systems.[82b] The AT^-/BAT redox couple showed better matching ability than the conventional polysulfide redox couple with the Pt, CoS or PEDOT CEs, and the PEDOT CE exhibited higher catalytic activity than Pt and CoS. A PCE of 1.53% was achieved for the QDSCs using PEDOT CE combined with the AT^-/BAT redox couple. Moreover, with the PEDOT CE, it was found that the QDSCs based on AT^-/BAT redox couple outperformed the QDSCs based on the T^-/T_2 redox couple due to the suppressed charge recombination.

The above mentioned metal sulfides and carbide belong to binary inorganic compounds (comprising two elements), whereas multiple compounds comprising three or more elements have also been introduced into QDSCs as CE catalysts. In a previous study,[75a] Lee et al. prepared $CuSnS_3$ (Fig. 11c) to catalyze the redox reaction of S^{2-}/S_x^{2-} in QDSC systems and the device gave a PCE of 4.06%, higher than the conventional copper sulfide CE. The Wang group synthesized porous Cu_2ZnSnS_4 and $Cu_2ZnSnSe_4$ with a simple spray method to be used as CEs in QDSCs.[83a] With the CdSe quantum dot based photoanode, the devices using Cu_2ZnSnS_4 and $Cu_2ZnSnSe_4$ CEs achieved PCEs of 2.19 and 4.35%. The higher performance of $Cu_2ZnSnSe_4$ over Cu_2ZnSnS_4 can be attributed to the intrinsic nature of $Cu_2ZnSnSe_4$ as well as the porous structure of the catalytic film formed under the high sinter temperatures, confirmed by SEM and EIS measurements. Using a pyrolysis procedure, Shi et al. prepared a porous structured Cu_2ZnSnS_4 thin film with pore sizes of 100-200 nm for CEs in QDSCs. After optimization, the device yielded a PCE of 2.56%.[83b] Lee et al. prepared a class of $Cu_2ZnSn(S_{1-x}Se_x)_4$ nanocrystals with different S/Se ratios (x = 0, 0.2, 0.5, 0.85, and 1) and investigated the impact of those ratios on catalytic activity.[83c] Firstly, all of the $Cu_2ZnSn(S_{1-x}Se_x)_4$ samples exhibited higher catalytic activity than Pt toward the regeneration of S^{2-}/S_x^{2-}. Secondly, the ratios of S/Se were found to play a crucial role in determining the catalytic activities for the redox reaction of S^{2-}/S_x^{2-}, confirmed by linear sweep voltammetry (LSV) and EIS, which revealed that the electron transfer kinetics and diffusion resistance of the electrolyte were related to the S/Se ratios. As a result, the device with $Cu_2ZnSn(S_{1-x}Se_x)_4$ where x = 0.5 as the CE achieved the highest PCE of 3.01%, much higher than the devices using other S/Se ratios. Xiao et al. compared the performance of a hollow $NiCo_2S_4$ single crystalline nanorod array and amorphous $NiCo_2S_4$ toward the S^{2-}/S_x^{2-} redox couple in QDSCs.[83d] The EIS experiments showed that the R_{ct} of the hollow $NiCo_2S_4$ CE was 11.9 Ω, lower than the amorphous $NiCo_2S_4$, indicating that the hollow $NiCo_2S_4$ CE exhibited better catalytic activity while the QDSCs yielded a PCE of 4.22%. The excellent behavior of hollow $NiCo_2S_4$ can be ascribed to the large catalytic active area, facilitated electrolyte transport, and the single crystalline 1D nanostructure which promotes fast electron transport, as evidenced by the different capacitance values in EIS and by the SEM images.

Au deposited on reduced graphene (RG) generated a composite Au/RG CE catalyst for QDSCs. The RG/Au composite CE showed a higher catalytic behavior than conventional Au or Pt CEs due to the ideal combination of the high catalytic activity of Au and the conductivity of the RG network structure. This device showed a PCE of 1.36%.[84] Song et al. deposited Cu_2S nanocrystals on the surface of ITO nanowire to form a Cu_2S/ITO composite as a CE for QDSCs.[85a] The QDSCs with this ITO/Cu_2S composite CE demonstrated a PCE of 4.06%, much higher than the plain Cu_2S CE based device. The improved catalytic activity caused by the reduced sheet resistance of the CE facilitated electron transfer from the ITO to the Cu_2S

because of the high quality tunnel junctions with short carrier transport paths (less than 100 nm) between them. In addition, the 3D structure of the nanowire array provided more active catalytic sites and easy accessibility for the polysulfide redox couple, which led to a decreased R_{ct}, contributing to the high catalytic activity. Meanwhile, CuS nanoparticles were grown in a controlled fashion on carbon nanofibers (CuS/Cf, Fig. 11d) by combining the versatility of the electrospinning technique and a hydrothermal process.[85b] The combination of the high catalytic activity CuS nanoparticles and the good charge transport provided by the 3D nanofiber framework generated a very high catalytic activity. The QDSCs using this composite CE produced a PCE of 3.86%, much higher the traditional bare CuS CE based device. In the catalytic process, the CuS behaves as the main catalyst in the reduction of the oxidized polysulfide, while the carbon nanofibers provide the 3D framework, facilitating the charge transport.

The Meng group prepared a PbS/Cb composite CE with different PbS/Cb weight ratios.[86a] In these composite CE, PbS provided a large area of catalytic sites and Cb worked as an excellent electrical tunnel for fast electron transport from the external circuit to PbS surface. When the weight ratio of PbS/Cb was 10:1, the PbS/Cb composite showed the best catalytic activity and the QDSCs achieved a PCE of 3.91%. Furthermore, a durability test over 1000 h proved that the PbS/Cb composite CE was highly stable under the working conditions. PbS nanoparticles were also loaded on graphene sheets that had been pre-deposited on FTO glass, resulting in a graphene/PbS composite CE for CdS/CdSe QDSCs.[86b] Under standard conditions, the device showed a PCE of 2.63%, remarkably higher than those using PbS (1.28%) or graphene (0.23%) CEs.

Wang et al. fabricated a composite CE by combining PbS nanoparticles with ZnO nanorod arrays.[86c] Compared with planar CEs, the ZnO nanorod array framework presented a larger surface area able to load more PbS catalysts and resulting in easy accessibility of the electrolyte. Moreover, the 3D structure of the ZnO nanorod arrays provides an excellent electron pathway for shuttling electrons to PbS catalytic sites. As a result, the ZnO/PbS composite CEs exhibited much higher catalytic activity for polysulfide and the QDSCs yielded a PCE of 3.06%. Yuan et al. fabricated a CoS/graphene composite and found that the graphene played a crucial role in forming the nanostructure of the electrode, endowing it with a high specific surface area and further excellent catalytic activity toward the polysulfide redox couple. Consequently, the QDSCs using the CoS/graphene composite CE showed a PCE of 2.90%.[87a] Using CoS nanorod arrays on graphite paper (GP) as a composite CE, combined with a flexible ZnO photoanode, Pan et al. assembled a flexible QDSC.[87b] The CoS/GP composite CE showed high catalytic activity and exchange current density and lower R_{ct} toward the polysulfide redox couple with a PCE of 2.70%, higher than those of QDSCs using Pt (0.52%) and GP (0.71%) CEs. This work also provides a feasible path to fabricate flexible electrodes for DSCs.

Using the CBD technique, Lin et al. prepared a fiber shaped Co_9S_8/Cf CE which showed much higher catalytic ability toward the reduction of S_x^{2-} than the conventional Pt CE.[87c] Using this fiber shaped composite CE, the researchers assembled fiber shaped QDSCs, obtaining a PCE of 3.79%. As previously mentioned, CoS and NiS CEs showed decent catalytic activity toward the polysulfide redox couple. Gopi et al. prepared FTO/CoS/NiS and FTO/NiS/CoS composite CEs.[87d] Interestingly, the QDSCs with the FTO/CoS/NiS CE exhibited a PCE of 3.40%, much higher than the device using FTO/NiS/CoS (2.53%). The photovoltaic difference is caused by the different values of R_s, the electron transport resistance, the mass transport resistance and the R_{ct} at the composite CEs. The Meng group introduced a ternary compound of $CuInS_2$ to QDSCs as a CE,[88a] resulting in a PCE of 3.63%. After adding an appropriate amount of Ca/Cb mixture to the $CuInS_2$ electrode, they achieved a $CuInS_2$/Ca/Cb composite with improved catalytic activity and stability. After fixing the weight ratio of $CuInS_2$/Ca+Cb at 1:1, this device showed a high PCE of 4.32%. In addition, a long term stability test indicated that the $CuInS_2$/Ca/Cb composite CE exhibited good stability under the working conditions for 1000 h.

Using water soluble MWCNTs and $Cu_2ZnSnSe_4$(CZTSe) nanoparticles, the Chen group obtained CZTSe/MWCNT composites with different weight ratios.[88b] When the weight ratio of MWCNT/CZTSe was 0.1, the composite CE achieved optimal behavior and the device produced a PCE of 4.60%. Based on the assumption that the MWCNTs provide a fast electron transfer channel in combination with fast interfacial electron exchange through the catalytic active surface of the CZTSe, they proposed a "composite charge transmission" model to explain the differences in the catalytic activity of the composite CEs with various weight ratios. This study revealed potential low cost and high efficiency QDSCs. Shu et al. fabricated a PEDOT/TiO_2 composite CE by an electro-polymerization method with different deposition charge capacities of 40, 80, 120, 160 mC cm^{-2}.[89] The QDSCs with the composite CE prepared at 120 mC cm^{-2} achieved a PCE of 1.56%. The higher catalytic activity was mainly due to the increased active surface area without the formation of large pores and aggregation under middle deposition charge capacities. The experimental conditions and results of the QDSCs using different counter electrode catalysts are summarized in Table S8.

The redox couples in QDSCs are not developing as fast as those in DSC systems and the most widely used redox couple is still polysulfide. The developments in CE materials are more dramatic and include carbon materials, transition metal carbides, nitrides, sulfides, oxides, multiple compounds, and composites.

4. Conclusions and Perspectives

In summary, DSCs have made remarkable strides with novel Pt-free CE catalysts accompanied by iodide-free redox couples, overcoming the challenges of high prices, limited Pt reserves, and the absorption of short wavelength light and strong corrosion of the iodide redox couple. We have reviewed a number of Pt-free CE catalysts for various iodide-free redox

couples including inorganic, organic, and metal complex materials, among others. The Pt-free CE catalysts contain carbon materials, polymers, metal compounds, multiple compounds, and composite materials.

Among the Pt-free catalysts, carbon materials, such Ca, Cb, CNTs, and graphene, have the merits of low cost, mature preparation processes, high catalytic activities and considerable stability. We believe that carbon CEs are the most promising candidates in the commercial production of DSCs. Organic polymers are the ideal transparent flexible CEs because they have the advantages of transparency, low cost, availability, and high catalytic activity. Nevertheless, there remain some problems to be resolved, such as the development of a gentle method to prepare flexible polymer CEs at low temperature, the exploration of new polymers, improved stability, and so forth. To date, metal carbides, nitrides, oxides, sulfides, phosphides, selenides, and tellurides have been proposed as CE catalysts in DSCs, with most of them showing high catalytic activity. The main problem with this type of catalyst is that the synthesis procedures generally consume large amounts of energy. Thus, the exploration of new synthesis routes with lower consumption is necessary for metal compound CEs. Multiple compound CEs are newcomers, and their long-term stability must be evaluated under harsh conditions. We believe that an increasing number of multiple compound CEs will be introduced into DSCs. Composites are the main force in Pt-free CE catalysts, and all of the composite catalysts work better than their individual components. The fundamental reasons for the higher catalytic activity of composites and the role of each component should be further investigated.

It has been proven that a matching issue exists between CE catalysts and redox couples. Therefore, design ~~low cost~~ Pt and TCO-free CE, such as integrated carbon sheet, is a promising path to pursuit low cost DSCs with high efficiency. In this process, the researchers should note that every part of a DSCs correlates with each other and a slight variation in one part may affect the overall status. The realization of the industrialization of DSCs requires our comprehensive consideration of each component of DSCs.

In QDSC systems, a metal CE cannot be suitable for the widely used polysulfide redox couple. The commonly used CEs are transition sulfides, such as Cu_2S, CuS, FeS, NiS, CoS, etc. Carbon materials, polymers, multiple compounds and composite materials are used only sporadically. Redox couples in QDSCs show slow development and there are few reports about polysulfide-free redox couples compared to the iodide-free redox couples in DSC systems. Improving the PCE of QDSCs is the main task of current research in that area.

Acknowledgements

This research was supported by the National Natural Science Foundation of China (Grant No. 21303039, 51273032), Natural Science Foundation of Hebei Province (Grant No. B2015205163, B2013205171), Support Program for Hundred Excellent Innovation Talents from the Universities of Hebei Province, BR2-220).

Notes and references

1 A. Shah, P. Torres, R. Tscharner, N. Wyrsch and H. Keppner, *Science*, 1999, **285**, 692-698.

2 a) S. Mathew, A. Yella, P. Gao, R. Humphry-Baker, B. F. E. Curchod, N. Ashari-Astani, I. Tavernelli, U. Rothlisberger, Md. K. Nazeeruddin and M. Grätzel, *Nat. Chem.*, 2014, **6**, 242-247; b) M. Green, K. Emery, Y. Hishikawa, W. Warta and E. Dunlop, *Prog. Photovolt: Res. Appl.*, 2014, **22**, 701-710; c) M. Ye, X. Wen, M. Wang, J. Iocozzia, N. Zhang, C. Lin, Z. Lin, *Mater. Today*, 2005, **18**, 155-162.

3 I. Hod and A. Zban, *Langmuir*, 2014, **30**, 7264-7273.

4 K. Zhao, Z. Pan, I. Mora-Seró, E. Cánovas, H. Wang, Y. Song, X. Gong, J. Wang, M. Bonn, J. Bisquert, X. Zhong, *J. Am. Chem. Soc.*, 2015, **137**, 5602-5609.

5 a) B. O' Regan and M. Grätzel, *Nature*, 1991, **353**, 737-740; b) M. Grätzel, *Nature*, **2001**, *414*, 338-344; c) C. Grätzel and S. M. Zakeeruddin, *Mater. Today*, 2013, **16**, 11-18.

6 a) M. Wang, C. Grätzel, S. M. Zakeeruddin and M. Grätzel, *Energy Environ. Sci.*, 2012, **5**, 9394-9405; b) J. Wu, Z. Lan, J. Lin, M. Huang, Y. Huang, L. Fan, and G. Luo, *Chem. Rev.*, 2015, **115**, 2136-2173.

7 a) M. Wu, X. Lin, Y. Wang, L. Wang, W. Guo, D. Qi, X. Peng, A. Hagfeldt, M Grätzel and T. Ma, *J. Am. Chem. Soc.*, 2012, **134**, 3419-2428; b) M. Wu, Y. Lin, H. Guo, K. Wu and X. Lin, *Chem. Commun*., 2014, **50**, 7625-7627; c) M. Wu, H. Guo, Y. Lin, K. Wu, T. Ma and A. Hagfeldt, *J. Phys. Chem. C*, 2014, **118**, 12635-12631; d) M. Wu, X. Lin, L. Wang, W. Guo, Y. Wang, J. Xiao, A. Hagfeldt and T. Ma, *J. Phys. Chem. C*, 2011, **115**, 22598-22602; e) M. Wu, Y. Wang, X. Lin, N. Yu, L. Wang, L. Wang, A. Hagfeldt and T. Ma, *Phys. Chem. Chem. Phys*., 2011, **13**, 19298-19301; f) M. Wu, J. Bai, Y. Wang, A. Wang, X. Lin, L. Wang, Y. Shen, Z. Wang, A. Hagfeldt and T. Ma, *J. Mater. Chem.*, 2012, **22**, 11121-11127; g) L. Wang, W. Wu, Y. Gao and T. Ma, *Appl. Phys. Lett*., 2011, **98**, 221102; h) H. Zhou, Y. Shi, L. Wang, H. Zhang, C. Zhao, A. Hagfeldt and T. Ma, *Chem. Commun*., 2013, **49**, 7626-7628.

8 a) A. Hauch and A. Georg, *Electrochim. Acta*, 2001, **46**, 3457-3466; b) Y. Hou, D. Wang, X. H. Yang, W. Q. Fang, B. Zhang, H. F. Wang, G. Z. Lu, P. Hu, H. J. Zhao and H. G. Yang, *Nat. Commun.*, 2013, **4**, 1583.

9 a) M. Wu and T. Ma, *ChemSusChem*, 2012, **5**, 1343-1357; b) F. Hao, P. Dong, Q. Luo, J. Li, J. Lou and H. Lin, *Energy Environ. Sci.*, 2013, **6**, 2003-2019; c) M. Wu, Y. Lin, H. Guo, T. Ma and A. Hagfeldt, *J. Power Sources*, 2014, **263**, 154-157; d) M. Wu, X. Lin, Y. Wang, A. Hagfeldt and T. Ma, *Angew. Chem. Int. Ed*., 2011, **50**, 3520-3524.

10 C. Teng, X. Yang, C. Yuan, C. Li, R. Chen, H. Tian, S. Li, A. Hagfeldt and L. Sun, *Org. Lett.,* 2009, **11**, 5542-5545.

11 G. Oskam, B. V. Bergeron, G. J. Meyer and P. C. Searson, *J. Phys. Chem. B*, 2001, **105**, 6867-6873.

12 P. Wang, S. M. Zakeeruddin, J.-E. Moser, R. Humphry-Baker and M. Grätzel, *J. Am. Chem. Soc.*, 2004, **126**, 7164-7165.

13 L. Li, X. Yang, J. Zhao, J. Gao, A. Hagfeldt and L. Sun, *J. Mater. Chem.*, 2011, **21**, 5573-5575.

14 a) Z. Zhang, P. Chen, T. N. Murakami, S. M. Zakeeruddin and M. Grätzel, *Adv. Funct. Mater.*, 2008, **18**, 341-346; b) S. Cazzanti, S. Caramori, R. Argazzi, C. M. Elliott and C. A. Bignozzi, *J. Am. Chem. Soc*., 2006, **128**, 9996-9997; c) B. A. Gregg, F. Pichot, S. Ferrere and C. L. Fields, *J. Phys. Chem. B*, 2001, **105**, 1422-1429; d) H. Tian, L. Sun, *J. Mater. Chem*., 2011, **21**, 10592-10601; e) M. Cheng, X. Yang, C. Chen, J. Zhao, F, Zhang and L. Sun, *Phys. Chem. Chem. Phys.*, 2013, **15**, 15146-15151; f) M. Chen, X. Yang, F. Zhang, J. Zhao and L.

Sun, *Angew. Chem. Int. Ed.*, 2012, **51**, 9896-9899; g) M. Wang, N. Chamberland, L. Breau, J-E. Moser, R. Humphry-Baker, B. Marsan, S. M. Zakeeruddin and M. Grätzel, *Nat. Chem.*, 2010, **2**, 385-389; h) J. Burschka, V. Brault, S. Ahmad, L. Breau, M. K. Nazeeruddin, B. Marsan, S. K. Zakeeruddin and M. Grätzel, *Energy Environ. Sci*., 2012, **5**, 6089-6097.

15 a) K. M. Bratlie, H. Lee, K. Komvopoulos, P. D. Yang and G. A. Somorjai, *Nano Lett*., 2007, **7**, 3097-3101; b) W. P. Zhou, A. Lewera, R. Larsen, R. Masel, P. Bagus and A. Wieckowski, *J. Phys. Chem. B*, 2006, **110**, 13393-13398.

16 a) M. Wu, Y. Lin, H. Guo, W. Li, Y. Wang and X. Lin, *Nano Energy*, 2015, **11**, 540-549; b) F. Hao, P. Dong, J. Zhang, Y. Zhang, P. E. Loya, R. Hauge, J. Li, J. Lou and H. Lin, *Sci. Rep.*, 2012, **2,** 368; c) S. Pan, Z. Yang, H. Li, L. Qiu, H. Sun and H. Peng, *J. Am. Chem. Soc.*, *2013*, **135**, 10622-10625; d) H. Wu, Z. Lv, Z. Chu, D. Wang, S. Hou and D. Zou, *J. Mater. Chem*., 2011, **21**, 14815-14820.

17 J. Zhang, H. Long, S. G. Miralles, J. Bisquert, F. Fabregat-Santiago and M. Zhang, *Phys. Chem. Chem. Phys.*, 2012, **14**, 7131-7136.

18 a) X. Li, L. Liu, G. Liu, Y. Rong, Y. Yang, H. Wang, Z. Ku, M. Xu, C. Zhong and H. Han, *Adv. Func. Mater.*, 2013, **23**, 3344-3353; b) X. Li, Z. Ku, Y. Rong, G. Liu, L. Liu, T. Liu, M. Hu, Y. Yang, H. Wang, M. Xu, P. Xiang and H. Han, *Phys. Chem. Chem. Phys*., 2012, **14**, 14383-14390; c) Z. Ku, X. Li, G. Liu, H. Wang, Y. Rong, M. Xu, L. Liu, M. Hu, Y, Yang and H. Han, *J. Mater. Chem. A*, 2013, **1**, 237-240; d) G. Liu, X. Li, H. Wang, Y. Rong, Z. Ku, M. Xu, L. Liu, M. Hu, Y, Yang and H. Han, *Carbon*, 2013, **53**, 11-18; e) K. Funabiki, Y. Saito, M. Doi, K. Yamada, Y. Yoshikawa, K. Manseki, Y. Kubota and M. Matsui, *Tetrahedron*, 2014, **70**, 6312-6317.

19 a) H. Tian, X. Jiang, Z. Yu, L. Kloo, A. Hagfeldt, and L. Sun, *Angew. Chem. Int. Ed*., 2010, **49**, 7328-7331; b) H. Tian, Z. Xu, A. Hagfeldt, L. Kloo, L. Sun, *J. Am. Chem. Soc.*, 2011, **133**, 9413-9422.

20 D. Noureldine, T. Shoker, M. Musameh and T. Ghaddar, *J. Mater. Chem.*, 2012, **22**, 862-869.

21 a) D. Li, H. Li, Y. Luo, K. Li, Q. Meng, M. Armand, L. Chen, *Adv. Func. Mater*., 2010, **20**, 3358-3365; b) Y. Liu, J. R. Jennings, M. Parameswaran, Q. Wang, *Energy. Environ. Sci.*, 2011, **4**, 564-571.

22 W. Cho, D. Song, Y. Lee, H. Chae, Y. R. Kim, Y. B. Pyun, S. Nagarajan, P. Sudhagar, Y. S. Kang, *J. Mater. Chem. A* **2013**, *1*, 233-236.

23 a) T.W. Hamann, O. K. Farha and J. T. Hupp, *J. Phys. Chem. C*, 200**8**, **112**, 19756-19764; b) T. Daeneke, T.-H. Kwon, A. B. Holmes, N. W. Duffy, U. Bach and L. Spiccia, *Nat. Chem.*, 2011, **3**, 213-217; c) T. Daeneke, Y. Uemura, N. Duffy, A. Mozer, N. Koumura, U. Bach and L. Spiccia, *Adv. Mater.*, 2012, **24**, 1222-1225.

24 a) S. Hattori, Y. Wada, S. Yanagida and S. Fukuzumi, *J. Am. Chem. Soc.*, 2005, **127**, 9648-9654; b) Y. Bai, Q. Yu, N. Cai, Y. Wang, M. Zhang and P. Wang, *Chem. Commun.*, 2011, **47**, 4376-4378.

25 a) T. C. Li, A. M. Spokoyny, C. She, O. K. Farha, C. A. Mirkin, T. J. Marks and J. T. Hupp, *J. Am. Chem. Soc.*, 2010, **132**, 4580-4582; b) A. M. Spokoyny, T. C. Li, O. K. Farha, C. W. Machan, C. She, C. L. Stern, T. J. Marks, J. T. Hupp and C. A. Mirkin, *Angew. Chem. Int. Ed.,* 2010, **49**, 5339-5343.

26 K. Oyaizu, N. Hayo, Y. Sasada, F. Kato and H. Nishide, *Dalton Transactions*, 2013, **42**, 16090-16095.

27 I. R. Perera, A. Gupta, W. Xiang, T. Daeneke, T. Bach, R. A. Evans, C. A. Ohlin and L. Spiccia, *Phys. Chem. Chem. Phys.*, 2014, **16**, 12021-12028.

28 A. Yella, H. Lee, H. Tsao, C. Yi, A. Chandiran, M. Nazeeruddin, E. Diau, C. Yeh, S. Zakeeruddin and M. Grätzel, *Science*, 2011, **334**, 629-634.

29 S. Feldt, E. Gibson, E. Gabrielsson, L. Sun, G. Boschloo and A. Hagfeldt, *J. Am. Chem. Soc.*, 2010, **132**, 16714-16724.

30 S. A. Sapp, C. M. Elliott, C. Contado, S. Caramori, A. Bignozzi, *J. Am. Chem. Soc.*, 2002, **124**, 11215-11222.

31 L. Wang, E. Diau, M. Wu, H. Lu and T. Ma, *Chem. Commun.*, 2012, 48, 2600-2602.

32 F. Ghamouss, R. Pitson, F. Odobel, M. Boujtita, S. Caramori and C. Bignozzi, *Electrochim. Acta*, 2010, **55**, 6517-6522.

33 K. Aitola, J. Halme, S. Feldt, P. Lohse, M. Borghei, A. Kaskela, A. Nasibulin, E. Kauppinen, P. Lund, G. Boschloo and A. Hagfeldt, *Electrochim. Acta*, 2013, **111**, 206-209.

34 S. Feldt, E. Gibson, G. Wang, G. Fabregat, G. Boschloo and A. Hagfeldt, *Polyhedron*, 2014, **82**, 154-157.

35 a) L. Kavan, J. Yum and M. Grätzel, *Nano. Lett.*, 2011, **11**, 5501-5506; b) L. Kavan, J. Yum, M. Nazeeruddin and M. Grätzel, *ACS Nano*, 2011, **5**, 9171-9178.

36 J. Roy-Mayhew, G. Boschloo, A. Hagfeldt and I. Aksay, *ACS Appl. Mater. Interfaces*, 2012, **4**, 2794-2800.

37 L. Kavan, J. Yum and M. Grätzel, *ACS Appl. Mater. Interfaces*, 2012, **4**, 6999-7006.

38 Y. Li, H. Wang, Q. Feng, G. Zhou and Z. Wang, *ACS Appl. Mater. Interfaces*, 2013, **5**, 8217-8224.

39 M. Al-Mamun, J. Kim, K. Lee, Y. Ko, J. Lee, I. In, J. Lee, Y. Sung and S. Kim, *Synthetic Met.*, 2013, **177**, 77-81.

40 a) M. Stefik, J. Yum, Y. Hut and M. Grätzel, *J. Mater. Chem. A*, 2013, **1**, 4982-4987; b) M. Ju, J. Kim, H. Choi, I. Choi, S. Kim, K. Lim, J. Ko, J. Lee, I. Jeon, J. Baek and H. Kim, *ACS Nano*, 2013, **7**, 5243-5250.

41 S. Shukla, N. Loc, P. Boix, T. Koh, R. Prabhakar, H. Mulmudi, J. Zhang, S. Chen, C. Ng, C. Huan, N. Mathews, T. Sritharan and Q. Xiong, *ACS Nano*, 2014, **8**, 10597-10605.

42 Z. Wang, H. Xu, Z. Zhang, X. Zhou, S. Pang and G. Cui, *Chin. J. Chem.*, 2014, **32**, 491-497.

43 a) H. Tsao, J. Burschka, C. Yi, F. Kessler, M. Nazeeruddin and M. Grätzel, *Energy Environ. Sci.*, 2011, **4**, 4921-4924; b) S. Carli, E. Busatto, S. Caramori, R. Boaretto, R. Argazzi, C. Timpson and C. Bignozzi, *J. Phys. Chem. C*, 2013, **117**, 5142-5153; c) M. Kashif, J. Axelson, N. Duffy, C. Forsyth, C. Chang, J. Long, L. Spiccia and U. Bach, *J. Am. Chem. Soc.*, 2012, **134**, 16646-16653.

44 J. Yum, E. Baranoff, F. Kessler, T. Moehl, S. Ahmad, T. Bessho, A. Marchioro, E. Ghadiri, J. Moser, C. Yi, M. Nazeeruddin and M. Grätzel, *Nat. Commun.*, 2012, **3**, 631.

45 H. Wang, Q. Feng, F. Gong, Y. Li, G. Zhou and Z. Wang, *J. Mater. Chem. A*, 2013, **1**, 97-104.

46 W. Zhang, Y. Cheng, X. Yin and B. Liu, *Macromol. Chem. Phys.*, 2011, **212**, 15-23.

47 a) K. Tennakone, G. R. R. A. Kumara, A. R. Kumarasinghe, K. G. U. Wijayantha and P. M. Sirimanne, *Semicond. Sci. Technol.*, 1995, **10**, 1689-1693; b) B. O'Regan and D. T. Schwartz, *Chem. Mater.*, 1998, **10**, 1501-1509; c) J. Bandara and H. Weerasinghe, *Sol. Energy Mater. Sol. Cells*, 2005, **85**, 385-390.

48 a) W. Zhang, R. Zhu, F. Li, Q. Wang and B. Liu, *J. Phys. Chem. C*, 2011, **15**, 7038-7043; b) B. Xu, E. Sheibani, P. Liu, J. Zhang , H. Tian, N. Vlachopoulos, G. Boschloo, L. Kloo, A. Hagfeldt and L. Sun, *Adv. Mater.*, 2014, **26**, 6629-6634.

49 U. Bach, D. Lupo, P. Comte, J. E. Moser, F. Weissortel, J. Salbeck, H. Spreitzer and M. Grätzel, *Nature*, 1998, **395**, 583-585.

50 J. Burschka, A. Dualeh, F. Kessler, E. Baranoff, N. L. Cevey-Ha, C. Yi, M. K. Nazeeruddin and M. Grätzel, *J. Am. Chem. Soc.*, 2011, **133**, 18042-18045.

51 a) B. Xu, H. Tian, D. Bi, E. Gabrielsson, E. M. J. Johansson, G. Boschloo, A. Hagfeldt and L. Sun, *J. Mater. Chem. A*, 2013, **1**, 14467-14470.

52 a) S. X. Tan, J. Zhai, M. X. Wan, L. Jiang and D. B. Zhu, *Synth. Met.*, 2003, **137**, 1511-1512; b) K. Murakoshi, R. Kogure, Y. Wada and S. Yanagida, *Chem. Lett.*, 1997, 471-472; c) D.

Gebeyehu, C. J. Brabec, N. S. Sariciftci, D. Vangeneugden, R. Kiebooms, D. Vanderzande, F. Kienberger and H. Schindler, *Synth. Met.*, 2002, **125**, 279-287; d) J. Li, T. Osasa, Y. Hirayama, T. Sano, K. Wakisaka and M. Matsumura, *Jpn. J. Appl. Phys.*, 2006, **45**, 8728-8732.

53 I. Chung, B. Lee, J. He, R. Chang and M. G. Kanatzidis, *Nature*, 2012, **485**, 486-490.

54 G. R. A. Kumara, S. Kaneko, M. Okuya and K. Tennakone, *Langmuir*, 2002, **18**, 10493-10495.

55 a) L. Schemidt-Mende, U. Bach, R. Humphy-Baker, T. Horiuchi, H. Miura, S. Ito, S. Uchida and M. Grätzel, *Adv. Mater.*, 2005, **17**, 813-815. b) C. Xu, J. Wu, U. V. Desai and D. Gao, *Nano Lett.*, 2012, **12**, 2420-2424.

56 X. Liu, W. Zhang, S. Uchida, L. Cai, B. Liu and S. Ramakrishna, *Adv. Mater.*, 2010, **22**, E150-E155.

57 Z. Xue, L. Wang, W. Liu and B. Liu, *Renew. Energy*, 2014, **72**, 22-28.

58 J. K. Koh, J. Kim, B. Kim, J. H. Kim and E. Kim, *Adv. Mater.*, 2011, **23**, 1641-1646.

59 H. J. Snaith, A. J. Moule, C. Klein, K. Meerholz, R. H. Friend and M. Grätzel, *Nano Lett.*, 2007, **7**, 3372-3376.

60 a) C. Girotto, B. P. Rand, S. Steudel, J. Genoe and P. Heremans, *Org. Electron.*, 2009, **10**, 735-740.b) S. K. Hau, H. L. Yip, K. Leong and A. K. Y. Jen, *Org. Electron.*, 2009, **10**, 719-723.

61 B. E. Hardin, W. Gaynor, I-K. Ding, S.-B. Rim, P. Peumans and M. D. McGehee, *Org. Electron.*, 2011, **12**, 875–879.

62 G. Y. Margulis, M. G. Christoforo, D. Lam, Z. M. Beiley, A. R. Bowring, C. D. Bailie, A. Salleo and M. D. McGehee, *Adv. Energy Mater.*, 2013, **3,** 1657-1663.

63 B. O'Regan, F. Lenzmann, R. Muis and J. Wienke, *Chem. Mater.*, 2002, **14**, 5023-5029.

64 H. Sakamoto, S. Igarashi, M. Uchida, K. Niume and M. Nagai, *Org. Electron.*, 2012, **13**, 514-518.

65 H. Wang, G. Liu, X. Li, P. Xiang, Z. Ku, Y. Rong, M. Xu, L. Liu, M. Hu, Y. Yang, H. Han, *Energy Environ. Sci.*, 2011, **4**, 2025-2029.

66 M. Xu, G. Liu, X. Li, H. Wang, Y. Rong, Z. Ku, M. Hu, Y. Yang, L. Liu, T. Liu, J. Chen and H. Han, *Org. Electron.*, 2013, **14**, 628-634.

67 J. Xia, C. Yuan and S. Yanagida, *ACS Appl. Mater. Inter.*, 2010, **2**, 2136-2139.

68 Y.-F. Chiang, C.-H. Tsai, P. Chen and T.-F. Guo, *Sol. Energy*, 2012, **86**, 1967-1972.

69 Y. Yang, K. Ri, Y. Rong, L. Liu, T. Liu, M. Hu, X. Li and H. Han, *Phys. Chem. Chem. Phys.*, 2014, **16**, 17743-17747.

70 H. K. Jun, M. A. Careen and A. K. Arof, *Renew. Sust. Energy Reviews*, 2013, **22**, 148-167.

71 G. Hodes, J. Manassen and D. Cahen, *J. Electrochem. Soc.*, 1980, **127**, 544-549.

72 a) V. Dao, Y. Choi, K. Yong, L. L. Larina, O. Shevaleevskiy and H. Choi, *J. Power. Source*, 2015, doi: 10.1016/j.jpowsour.2014.10.095; b) C. Justin, Raj, K. Prabakar, A. D. Savariray and H. Kim, *Electrochim. Acta*, 2013, **103**, 231-236; c) Z. Ning, C. Yuan, H. Tian, Y. Fu, L. LI, L. Sun and H. Ågren, *J. Mater. Chem.*, 2012, **22**, 6032-6037; d) Z. Ning, H. Tian, C. Yuan, Y. Fu, L. Li, L. Sun and H. Ågren, *Chem. Eur. J.*, 2011, **17**, 6330-6333; e) A. J. Haring, M. E. Pomatto, M. R. Thornton and A. Morris, *ACS Appl. Mater. Interfaces*, 2014, **6**, 15061-15067.

73 a) A. Braga, S. Giménez, I. Concina, A. Vomiero and I. Mora-Seró, *J. Phys. Chem. Lett.*, 2011, **2**, 454-460; b) P. K. Santra and P. V. Kamat, *J. Am. Chem. Soc.*, 2012, **134**, 2508-2511; c) I. V. Lightcap and P. V. Kamat, *J. Am. Chem. Soc.*, 2012, 134, 7109-7116; d) Z. Pan, K. Zhao, H. Zhang, Y. Feng and X. Zhong, *ACS Nano*, 2013, **7**, 5215-5222.

74 a) K. Zhao, H. Yu, H. Zhang and X. Zhong, *J. Phys. Chem. C*, 2014, **118**, 5683-5690; b) W. Ke, G. Fang, H. Lei, P. Qin, H. Tao, W. Zeng, J. Wang and X. Zhao, *J. Power Sources*, 2014, **248**, 809-815; c) C. Shen, L. Sun, Z. Yu and Q. Wang, *J. Mater. Chem. A*, 2014, **2**, 2807-2813; d) Y. Yang, Q. Zhang, T. Wang, L. Zhu, X. Huang, Y. Zhang, X. Hu, D. Li and Q. Meng, *Electrochim. Acta*, 2013, **88**, 44-50; e) Z. Peng, Y. Liu, Y. Zhao, K. Chen, Y. Cheng and W. Chen, *Electrochim. Acta*, 2014, **135**, 276-283.

75 a) J. Xu, X. Yang, T. Wong and C. Lee, *Nanoscale*, 2012, **4**, 6537-6542; b) S. S. Kalanur, S. Y. Chae and O. S. Joo, *Electrochim. Acta*, 2013, **103**, 91-95; c) I. Lim, D. Y. Lee, S. A. Patil, N. K. Shrestha, S. H. Kang, Y. Nah, W. Lee and S. Han, *Mater. Chem. Phys.*, 2014, **148**, 562-568.

76 a) Z. Tachan, M. Shalom, I. Hod, S. Rühle, S. Tirosh and A. Zaban, *J. Phys. Chem. C*, 2011, **115**, 6162-6166; b) B. Kim, M. Son, S. Kim, N. Hong, S. Park, M. Jeong, H. Seo, K. Prabakar and H. Kim, *Electrochim. Acta*, 2014, **117**, 92-98.

77 a) H. Kim, T. Yeo, S. Kim, S. S. Rao, A. D. Savariraj, K. Prabakar and C. V. V. M. Gopi, *Eur. J. Inorg. Chem.*, 2014, 4281-4286; b) H. Kim, D. Kim, S. S. Rao, A. D. Savariraj, K. Kyoung, M. Son, C. V. V. M. Gopi and K. Prabakar, *Electrochim Acta*, 2014, **127**, 427-432.

78 a) J. Xu, H. Xue, X. Yang, H. Wei, W. Li, Z. Li, W. Zhang and C. Lee, *Small*, 2014, **10**, 4754-4759; b) L. Quan, W. Li, L. Zhu, H. Geng, X. Chang and H. Liu, *J. Power Sources*, 2014, **272**, 546-553; c) H. Chen, L. Zhu, H. Liu and W. Li, *J. Power Sources*, 2014, **245**, 406-410.

79 a) S. T. Finn and J. E. Macdonald, *Adv. Energy Mater.*, 2014, **4**, 1400495; b) H. Yu, H. Bao, K. Zhao, Z. Du, H. Zhang and X. Zhong, *J. Phys. Chem. C*, 2014, **118**, 16602-16610; c) N. Balis, V. Dracopoulos, K. Bourikas and P. Lianos, *Electrochim. Acta*, 2013, **91**, 246-252; d) H. Chen, L. Zhu, H. Liu and W. Li, *J. Phys. Chem. C*, 2013, **117**, 3739-3746.

80 a) W. Guo, Y. Shen, M. Wu, L. Wang, L. Wang and T. Ma, *Chem. Eur. J.*, 2012, 18, 7862-7868; b) D. H. Youn, M. Seol, J. Y. Kim, J. Jang, Y. Choi, K. Yong and J. S. Lee, *ChemSusChem*, 2013, **6**, 261-267.

81 a) S. Fan, B. Fang, J. H. Kim, B. Jeong, C. Kim, J. Yu and J. Ko, *Langmuir*, 2010, **26**, 13644-13649; b) G. S. Paul, J. H. Kim, M. Kim, K. Do, J. Ko and J. Yu, *ACS Appl. Mater. Interfaces*, 2012, **4**, 375-381; c) P. Sudhagar, E. Ramasamy, W. Cho, J. Lee and Y. S. Kang, *Electrochem. Commun.*, 2011, **13**, 34-37; d) M. Seol, E. Ramasamy, J. Lee and K. Yong, *J. Phys. Chem. C*, 2011, **115**, 22018-22024; e) V. Ganapathy, E. Kong, Y. Park, H. M. Jang and S. Rhee, *Nanoscale*, 2014, **6**, 3296-3301; f) J. Dong, S. Jia, J. Chen, B. Li, J. Zheng, J. Zhao, Z. Wang and Z. Zhu, *J. Mater. Chem.*, 2012, **22**, 9745-9750.

82 a) M. Yeh, C. Lee, C. Chou, L. Lin, H. Wei, C. Chu, R. Vittal and K. Ho, *Electrochim. Acta*, 2011, **57**, 277-284; b) T. Shu, X. Li, Z. Ku, S. Wang, S. Wu, X. Jin and C. Hu, *Electrochim. Acta*, 2014, **137**, 700-704.

83 X. Zeng, W. Zhang, Y. Xie, D. Xiong, W. Chen, X. Xu, M. Wang and Y. Cheng, *J. Power Sources*, 2013, **226**, 359-362; b) Y. Zhang, C. Shi, X. Dai, F. Liu, X. Fang and J. Zhu, *Electrochim. Acta*, 2014, **118**, 41-44; c) Y. Cao, Y. Xiao, J. Jung, H. Um, S. Jee, H. M. Choi, J. H. Bang and J. Lee, *ACS App. Mater. Interfaces*, 2013, **5**, 479-484; d) J. Xiao, X. Zeng, W. Chen, F. Xiao and S. Wang, *Chem. Commun.*, 2013, **49**, 11734-11736.

84 G. Zhu, L. Pan, H. Sun, X. Liu, T. Lv, T. Lu, J. Yang and Z. Sun, *ChemPhysChem*, 2012, **13**, 769-773.

85 a) Y. Jiang, X. Zhang, Q. Ge, B. Yu, Y. Zou, W. Jiang, W. Song, L. Wan and J. Hu, *Nano Lett.*, 2014, **14**, 365-372; b) L. Li, P. Zhu, S. Peng, M. Srinivasan, Q. Yan, A. S. Nair, B. Liu and S. Samakrishna, *J. Phys. Chem. C*, 2014, **118**, 16526-16535.

86 a) Y. Yang, L. Zhu, H. Sun, X. Huang, Y. Luo, D. Li and Q. Meng, *ACS Appl. Mater. Interfaces*, 2012, **4**, 6162-6168; b) P. Parand, M. Samadpour, A. Esfandiar and A. I. Zad, *ACS Photonics*, 2014, **1**, 323-330; c) X. Song, M. Wang, J. Deng, Y. Ju, T. Xing, J. Ding, Z. Yang and J. Shao, *J. Power Sources*, 2014, **269**, 661-670.

87 a) H. Hu, J. Ding, J. Qian, Y. Li, L. Bai and N. Yuan, *Mater. Lett.*, 2014, **114**, 7-10; b) M. Que, W. Guo, X. Zhang, X. Li, Q. Hua, L. Dong and C. Pan, *J. Mater. Chem. A*, 2014, **2**, 13661-13666; c) W. Guo, C. Chen, M. Ye, M. Lv and C. Lin, *Nanoscale*, 2014, **6**, 3656-3663; d) H. Kim, S. Kim, C. V. V. M. Gopi, S. Kim, S. S. Rao and M. Jeong, *J. Power Sources*, 2014, **268**, 163-170.
88 a) X. Zhang, X. Huang, Y. Yang, S. Wang, Y. Gong, Y. Luo, D. Li, and Q. Meng, *ACS Appl. Mater. Interfaces*, 2013, **5**, 5954-5960; b) X. Zeng, D. Xiong, W. Zhang, L. Ming, Z. Xu, Z. Huang, M. Wang, W. Chen and Y. Cheng, *Nanoscale*, 2013, **5**, 6992-6998
89 T. Shu and Z. Ku, *J. Alloy. Compd.*, 2014, **586**, 257-260.